

Chapter 3

Selection of Optimal Pulse Sequences for fMRI

Mark J. Lowe and Erik B. Beall

Summary

In this chapter, we discuss technical considerations regarding pulse sequence selection and sequence parameter selection that can affect fMRI studies. The major focus is on optimizing MRI data acquisitions for blood oxygen level-dependent signal detection. Specific recommendations are made for generic 1.5-T and 3.0-T MRI scanners.

Key words: MRI, fMRI, Pulse sequences, Blood oxygen level dependent, Echo-planar imaging, Spiral imaging

MRI signals are generated by exposing nuclei placed in a static magnetic field to radiofrequency (RF) pulses in the presence of rapidly switching magnetic field gradients. These patterns of RF pulses and magnetic field gradients are referred to as *pulse sequences*. Pulse sequences dictate the contrast that will be present in MR images.

The issue of optimal pulse sequences, or more generally, optimal data acquisition strategies for functional neuroimaging, is a complex one. One cannot categorically say that a particular approach is superior to any other in all cases. In this chapter, we will examine the issues that affect the detection sensitivity of neuronal activation in MRI and discuss relevant data acquisition strategies that can be optimal in each situation. For those readers who are not interested in the technical details involved in fMRI pulse sequence optimization and who wish to simply read a summary of recommended pulse sequence strategies for blood oxygen level-dependent (BOLD) fMRI, it is recommended that they skip to **Section 5**, which summarizes the

issues and presents recommendations and caveats for each relevant sequence parameter.

1. Physics of Functional Contrast in MRI

With a few notable exceptions, such as diffusion-weighted MRI, MRI contrast stems from taking advantage of the different MR relaxation rates in different tissues and in the presence of pathology. Felix Bloch phenomenologically characterized the dynamic evolution of spin magnetization with two time constants, referred to as T_1 and T_2 . An in-depth discussion of the Bloch equations is beyond the scope of this chapter, but for the purposes of understanding the interaction of pulse sequence parameters and functional contrast in MRI, it is useful to briefly describe the processes associated with these relaxation time constants.

T_1 relaxation is taken to be the time constant of the return of an excited ensemble of nuclei to the equilibrium state of the “lattice” or surroundings. So, before excitation, the ensemble will generally be in equilibrium with its surroundings. After excitation, T_1 governs the time for it to return to the state of equilibrium with the lattice. This is sometimes referred to as spin–lattice relaxation.

T_2 relaxation, which is technically an enhancement of T_1 relaxation (i.e., the upper limit of T_2 is T_1), is the time constant for an excited ensemble of nuclei to lose phase coherence through interactions with each other. This is sometimes referred to as spin-spin relaxation. T_2 relaxation in solids and tissue is typically much faster than T_1 .

For functional imaging, another important parameter governing relaxation is T_2^* , which is an enhancement of T_2 caused by magnetic field gradients inhomogeneities. T_2^* is defined as

$$\frac{1}{T_2^*} = \frac{1}{T_2} + \frac{1}{T_2'}, \quad (1)$$

where T_2' is the additional relaxation contribution from field inhomogeneities.

These relaxation processes are sensitive to the chemical environment of the nuclei. MRI utilizes this fact to produce images whose contrast is based on the different relaxation rates in different tissues.

1.1. Magnetic Resonance Relaxometry

Exposing nuclei in a static magnetic field to RF radiation at the Larmor frequency, given by

$$\nu_L = \gamma B \quad (2)$$

will result in the absorption of energy by the nuclei. In **Eq. 2**, γ is the gyromagnetic ratio and is a property of the nucleus. Since B is the static field strength, we see from **Eq. 2** that the Larmor frequency will rise linearly with field strength. For protons, $\gamma = 42.58 \text{ MHz/T}$ so the Larmor frequency at 1.5 T is approximately 64 MHz.

When the RF radiation is stopped, the nuclei will gradually release the energy into the surrounding material until they return to the pre-excited state of equilibrium with their surroundings.

An MR pulse sequence is characterized mainly by two parameters that control the contrast of the acquired data. The first is called the repetition time, or TR, which dictates how frequently the nuclei in a particular location are excited. If they are excited much more rapidly than the T_1 relaxation rate of the tissue, the protons will not recover to equilibrium between excitations. After a few excitations, the nuclei in a given location will approach a steady state. **Figure 1** shows an example of the signal evolution in tissue with different T_1 as a function of TR.

The other important parameter that is used to control contrast is the echo time, or TE. This is the time after excitation that the observed signal is spatially encoded. The amount of signal that can be spatially encoded is dictated by both TR and TE. Two of the most common methods for refocusing MR signal to allow spatial encoding are the spin echo (SE) and the gradient recalled echo (GRE) methods.

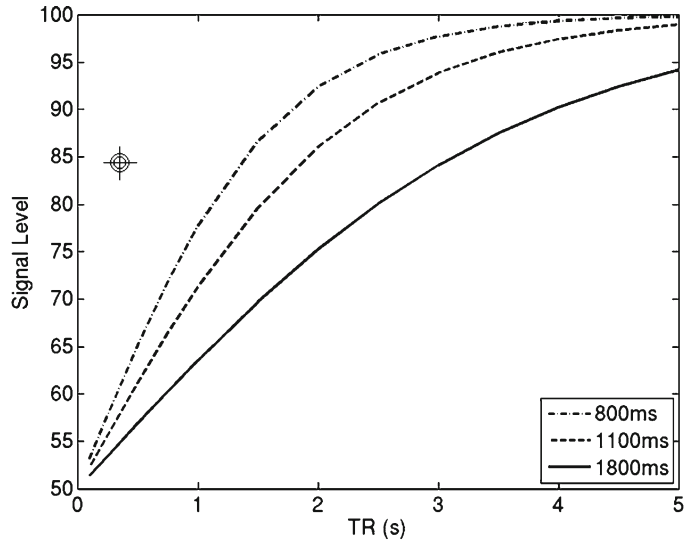


Fig. 1. Steady-state MR signal as a function of repetition time (TR) for tissue with three different T_1 relaxation times.

1.1.1. The Spin Echo

The time evolution of MR signal immediately after excitation is referred to as free induction decay (FID) in MR. During the FID, the processes governing the loss of signal coherence are a combination of T_1 , T_2 , and T_2' -related processes. In tissue, T_2' will have a large effect on the loss of signal. T_2' effects are what are referred to as reversible processes. The loss of phase coherence from these effects can be reversed by applying a refocusing RF pulse. **Figure 2** illustrates the sequence timing, using a pulse sequence timing diagram. Application of a refocusing RF pulse at a time t after the initial excitation pulse will result in a complete refocusing of the reversible dephasing effects at a time $2t$. This is referred to as a spin echo. The time $2t$ is usually called the echo time or TE. The MR signal from a given pulse sequence can be derived from the Bloch equations. For a SE acquisition, the MR signal will be given by

$$S_{SE} \propto \exp\left(\frac{-TE}{T_2}\right) \left\{ 1 - 2\exp\left(-\frac{TR - \frac{TE}{2}}{T_1}\right) + \exp\left(\frac{-TR}{T_1}\right) \right\}. \quad (3)$$

As is clear from **Eq. 3**, the MR signal from a SE acquisition is moderated by T_1 and T_2 . From this we can see that the T_2 will affect the encoded signal if the TE is comparable to, or longer than T_2 . **Figure 3** shows an example of the signal evolution for different TEs and T_2 s.

1.1.2. The Gradient Recalled Echo

It is possible to perform the spatial encoding for MRI during the FID. An echo can be created by increasing the dephasing

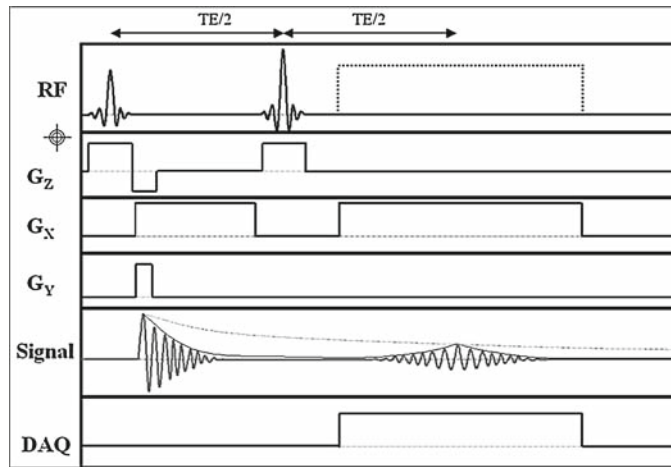


Fig. 2. Pulse sequence diagram of a spin-echo acquisition. The envelope of the signal indicates the free induction decay (FID), while the peak of the echo is modulated by T_2 according to **Eq. 3**.

through application of a brief field gradient along a particular direction and then reversing it while acquiring the signal data. This is called a GRE or a field echo.¹ The sequence diagram for this technique is shown in **Fig. 4**. The signal obtained from a GRE acquisition is given by

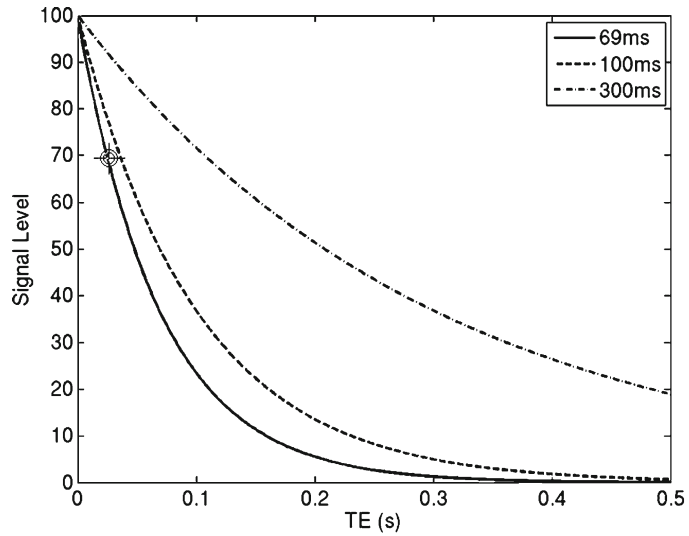


Fig. 3. Steady-state MR signal as a function of echo time (TE) for tissue with three different T_2 relaxation times.

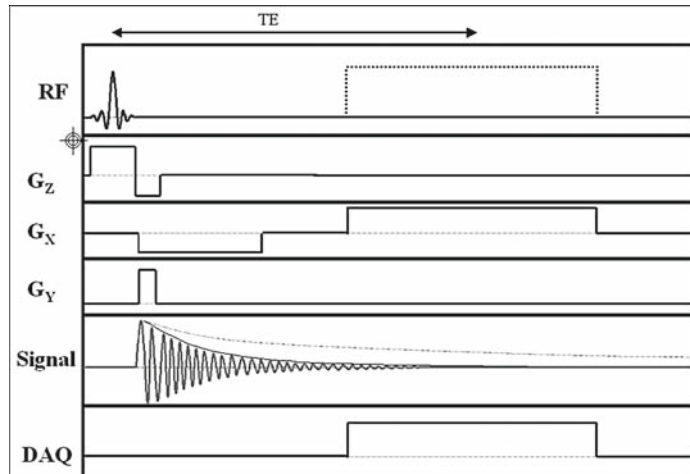


Fig. 4. Pulse sequence diagram of a gradient recalled echo acquisition.

¹This is sometimes shortened to gradient-echo (GE).

$$S_{\text{GRE}} \propto \exp\left(\frac{-\text{TE}}{T_2^*}\right) \sin \alpha \frac{1 - \exp\left(\frac{-\text{TR}}{T_1}\right)}{1 - \cos \alpha \exp\left(\frac{-\text{TR}}{T_1}\right)}, \quad (4)$$

where α is the flip angle, which is a sequence parameter that is a function of the amount of transmitted power.²

It can be shown from **Eqs. 3** and **4** that the TE that will maximize the difference in signal between two tissues with different T_2 or T_2^* is approximately the average of the T_2 s or T_2^* of the two tissue types. **Table 1** lists the T_1 and T_2 of gray matter and white matter in the human brain at 1.5 T and 3.0 T.

Historically, evidence of regionally specific functional contrast using MRI was first observed using an exogenous contrast agent (1). However, this observation was very quickly followed by several groups, employing the phenomenon of BOLD contrast observed by Ogawa and colleagues (2), utilizing endogenous contrast to observe brain activation in several different brain regions (3–6).

1.2. Exogenous Functional Contrast

It is possible to generate dynamic MR images with functional contrast by utilizing the fact that regional blood flow increases proximal to activated neurons. This is typically done by using methods similar to those used to measure regional blood perfusion with MRI. Gadolinium chelates will not cross the blood-brain barrier. Thus, a bolus injection of such a paramagnetic material will cause a transient change in the T_2 relaxation near arterial blood vessels that are perfusing brain tissue. If this is done while rapidly acquiring T_2^* -weighted MR images of the brain region that is active, one will observe a decrease in the measured signal intensity that is monotonically related to the volume of gadolinium passing

Table 1
Approximate relaxation times for gray and white matter at 1.5 T and 3.0 T

	1.5 (T)			3.0 (T)		
	T_1 (ms)	T_2 (ms)	T_2^* (ms)	T_1 (ms)	T_2 (ms)	T_2^* (ms)
White matter	600	80	70	800	70	60
Gray matter	900	100	60	1,100	90	50

²The flip angle can also affect the contrast of the generated images, but for simplicity, we focus here on the more intuitive parameters TE and TR.

through. One can infer directly the volume of blood perfusing this region from the signal decrease.

Functional contrast can thus be obtained in MRI by comparing the regional perfusion, measured with bolus contrast injection, while performing a task to that measured while at rest. **Figure 5** is an example of the difference in the MRI signal evolution from the same brain region in visual cortex while undergoing photic stimulation and in darkness. One can see that the area under the curve for photic stimulation is larger than that for rest, indicating that the volume of blood perfusing the tissue was increased during stimulation.

In this manner, one can produce voxel level comparisons of the area under the bolus passage curve in the MR time courses and determine those whose measured volume change was statistically significant.

Due to the invasive nature of the necessary bolus injection, the (albeit low level) risk of adverse reaction to contrast agents, the lower signal-to-noise ratio (SNR) of perfusion measurement techniques, and to a lesser extent, the limited volume coverage of perfusion measuring techniques, exogenous contrast-enhanced fMRI is only rarely performed and usually for reasons specific to a particular experimental design.

1.3. Endogenous Functional Contrast

There are two principal mechanisms for generating contrast in MR images using endogenous features related to neuronal activation. Both of these mechanisms are related to the hemodynamic response to an increase in neuronal activation. One of these is a regional increase in blood flow and the other is a concomitant

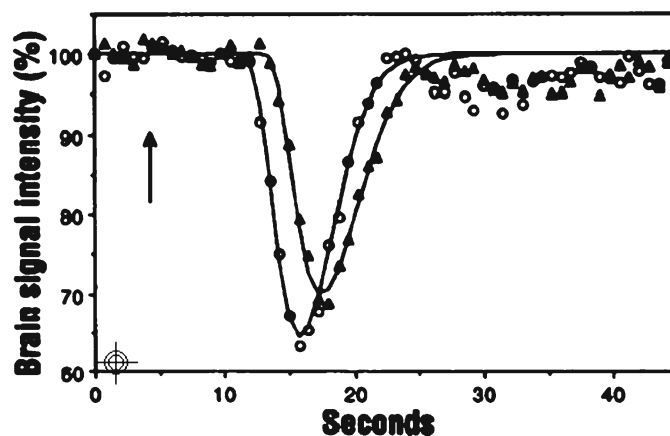


Fig. 5. Changes in MR brain signal intensity during the first-pass transit of intravenously administered paramagnetic contrast agent. *Open triangle* symbols represent the time course of signal during photic stimulation and *open circle* symbols represent the time course during rest (darkness). Reproduced with permission from (1).

increase in the oxygenation content of the blood perfusing tissue near activated neurons.

Far and away the most commonly employed fMRI acquisitions utilize the fact that regional brain activation results in a local increase in blood oxygenation. This is called BOLD contrast. The contrast in BOLD stems from the fact that oxygenated hemoglobin is a weakly diamagnetic molecule, while deoxygenated hemoglobin is a strongly paramagnetic molecule. The relative increase in the concentration of oxygenated hemoglobin in the vessels perfusing activated tissue results in an increase in the T_2 and T_2^* relaxation times in the affected brain regions. Thus, methods utilizing BOLD contrast for fMRI employ acquisition techniques that are sensitive to changes in T_2 and T_2^* . Because of the flexibility of T_2 and T_2^* acquisition methods, this has become the contrast of choice for the vast majority of fMRI experiments. For this reason, the remainder of this chapter will focus on acquisition strategies to acquire BOLD-weighted MRI data and we will discuss methods to optimize these depending on experimental needs.

2. Ultrafast Spatial Encoding

It is possible to generate MR images that will demonstrate a change in signal in brain regions that transition from the inactive to active state. These transitions are typically very rapid and the advantage of MRI over other imaging techniques is the ability to acquire even whole brain images very rapidly. In this section, we introduce the concept of spatial encoding in MRI and discuss the most common ultrafast imaging pulse sequences used in fMRI. For simplicity, throughout this section, we refer to the net magnetization within a sample as “spin.”

2.1. The Pulse Sequence

As stated above, the pulse sequence refers to the specific acquisition strategy in which spatial encoding and magnetization read-out is performed, providing the basic structure of the RF pulses and field gradients used. Because conventional MRI is based on Fourier spatial encoding, it has become convention within MRI to discuss pulse sequences in the context of k -space, another name for the Fourier conjugate of coordinate space. k -Space is essentially the image in the spatial frequency domain, and most pulse sequences acquire image data in this domain. There are a variety of advantages to this; most importantly that a coordinate space image can be produced simply by performing a two-dimensional Fourier transform (typically computed using the Fast Fourier Transform, or FFT) on sequentially acquired MRI data.

A pulse sequence for reading one arbitrary line of k -space with a gradient-recalled echo is shown in **Fig. 6**.

Starting with stage (1), waveforms are played out on the z -direction gradient, G_z , and the RF transmit channel to excite a slice of proton spins. During stage (2), the readout gradient (G_x) prewind and phase-encode gradient selection (G_y) is performed while rephasing spins across the slice/slab with G_z . During stage (3), the readout gradient is switched on while the emitted RF signal from the sample is recorded, denoted by the block of dotted lines. The diagrams shown are simplifications, where the timing and form of the gradients are changed according to various design considerations. The corresponding traversal of k -space for the pulse sequence in **Fig. 6** is shown in **Fig. 7**.

Typical conventional (i.e., not single-shot) sequences repeat this process, for different lines of k_y , or phase-encoding positions. This is shown in **Fig. 6**, step 2 with the G_y gradient at multiple possible values containing the variation in the repeated lines of k -space sampling. It should be noted that the distance traveled in k -space is proportional to the time integral of the gradient strength in space, so it is possible to use a larger amplitude to shorten the time taken to traverse k -space.³

The sequence described above pertains to a GRE, but without loss of generality, the same sequence applies to a SE sequence. A slice selective RF excitation pulse for both GRE and SE is typically a sinc function-shaped pulse, with amplitude set to rotate

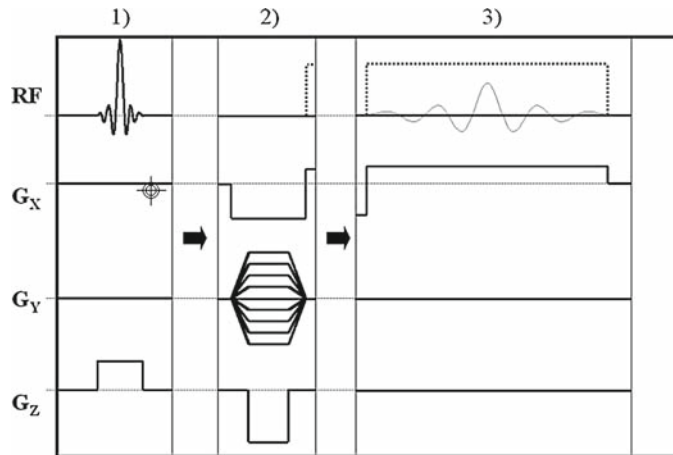


Fig. 6. Pulse sequence diagram for reading one line of k -space, time increases from *left* to *right*. The proton echo from the sample is shown here in *light gray* during and under the readout window, which will be sampled by a receive coil.

³Up to the limits of the gradient hardware and not without various drawbacks.

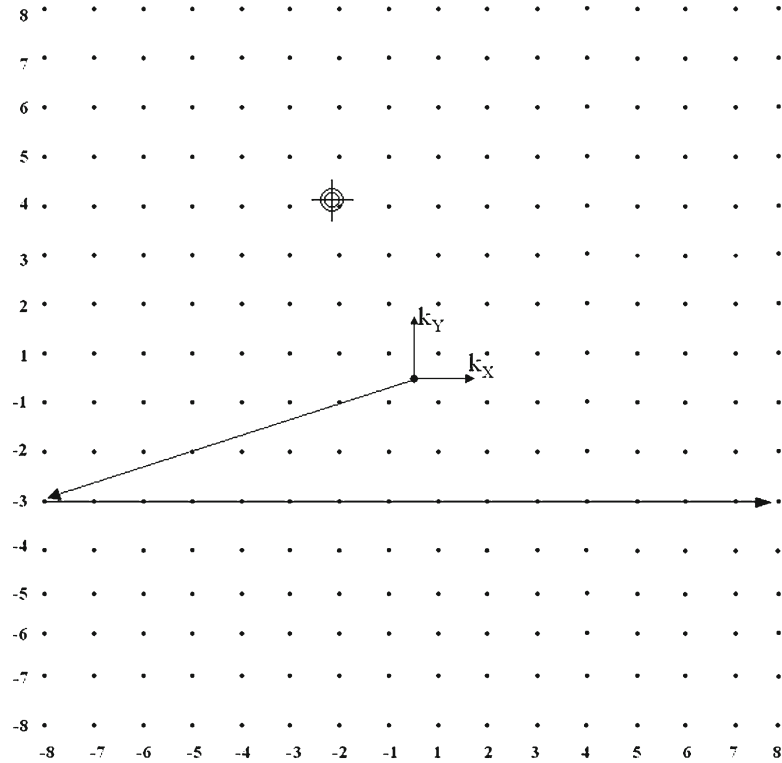


Fig. 7. k -Space diagram showing 16×16 matrix of data sampling points and trajectory of pulse sequence diagrammed in **Fig. 6**. k -Space is first prewound in step 2 (G_x moves position in k_x from 0 to -8 , G_y moves position in k_y from 0 down to line -3), then k_x is traversed in step 3 while sampling from -8 to $+8$.

the slice magnetization 90° from the longitudinal magnetization direction into the plane transverse to the static field. A SE sequence is very similar, but with the addition of a refocusing pulse set at 180° , timed to play out midway between the centers of the RF excitation pulse in step 1 and the readout window in step 3 in **Fig. 6**. The differences between SE and GRE can be seen in **Fig. 8**. The timing of the inversion pulse after the excitation pulse dictates the TE, so a short TE can preclude the SE method. SE can be advantageous because it can cancel dephasing due to local field inhomogeneities, leading to an improved SNR, but single-shot sequences get less of this benefit due to an effective spread of TEs which will be discussed later.

Strategies for what is referred to as “single-shot” imaging are critical to the high sampling rates necessary for dynamic imaging techniques such as fMRI. Echo-planar imaging (EPI) and spiral imaging are the most widely used of these. In addition, parallel imaging techniques, combined with the increasing use of multichannel coil technology, are playing an increasing role in fMRI.

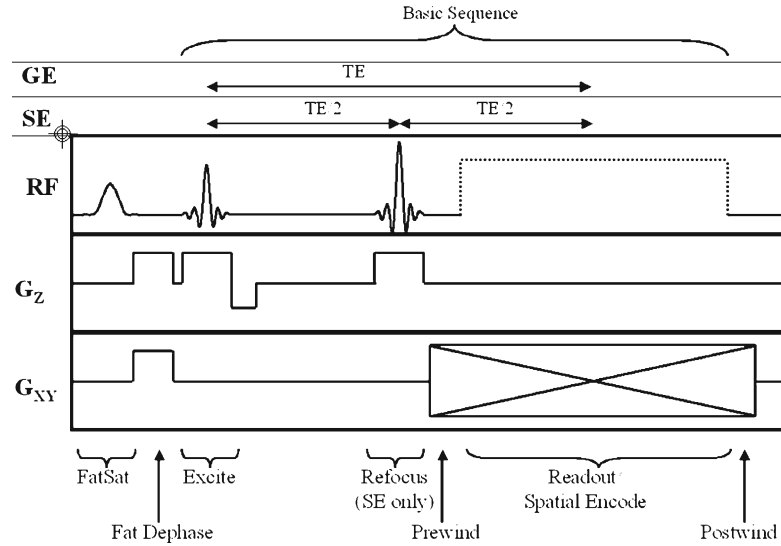


Fig. 8. Generalized diagram for either gradient-echo (GE) or spin-echo (SE) ultrafast pulse sequences specific to ultrafast imaging. A fat saturation pulse (described later), followed by excitation, then a refocus pulse (if spin-echo only), prewind gradients to set position in k -space, then the readout and spatial encoding gradients. Finally there may be postwind spoiler/crusher gradients (RF may also be used at the end) to dephase residual signal.

Single-shot sequences differ from conventional pulse sequences in that the data for an entire slice are acquired in one readout window after one excitation. This has been made possible by fast gradient switching technologies, and single-shot sequences are available on all modern MRI scanners. Common to all fast imaging sequences are higher demands on the hardware, which increase vibration and heating of the scanner, leading to increasing inhomogeneity and field drift over time during long scans (7, 8). Parallel imaging is a recent development, which reduces the readout time by acquiring data from multiple coils. These imaging strategies have various artifacts and tradeoffs, which will be discussed below following an introduction to the most common strategies.

2.2. Echo-Planar Imaging

EPI follows the basic strategy of excitation of a slice or slab followed by readout of one line (in the readout direction, or k_x) in k -space. The GRE sequence was shown in the pulse sequence timing diagram in Fig. 8 without the SE refocusing pulse, which was also shown in parts in Fig. 6. With the fast gradient switching speeds available in recent years, it has become possible to spatially encode an entire slice in one echo by performing multiple readouts and phase-encoding steps after a single excitation. The most common implementation, known as “Blipped EPI,” involves excitation of a slice followed by readout of k_x line like the

GRE sequence. The sequence continues, however, after an increment, or “blip,” of the position in k -space in the other dimension using a short-duration gradient pulse (in the phase-encode direction, or k_y). Readout continues when the readout gradient is reversed to read another k_x line in k -space immediately adjacent to the first line sampled but in the opposite direction. This is shown in **Fig. 9**.

These reversals and blips are repeated to adequately sample k -space and the resulting data can be treated in the same manner as multishot imaging, with the full readout of the slice or slab centered on the TE. The trajectory in k -space is shown in **Fig. 10**.

Three-dimensional acquisitions can be performed using an additional increment in the perpendicular dimension, or k_z , although most blipped-EPI sequences are two dimensional only due to the constraint of a shorter TE required. There exist many modifications to this basic structure, but all EPI strategies contain a fast back-and-forth cycling of the gradients to produce a GRE train. The blipped EPI strategy is commonly also referred to as Cartesian imaging, due to the rectangular trajectory of readout in k -space. We will not discuss other non-Cartesian strategies that are no longer common such as constant-phase encode (PE) EPI or square-spiral EPI. The signal generation stage before the spatial encoding can include a refocusing pulse or not, depending on whether T_2 (SE-EPI) or T_2^* (GRE-EPI) weighting is desired.

2.3. Spiral Imaging

Another common strategy for single-shot imaging is spiral imaging (9). In this scheme, k -space is sampled in a spiral or circular

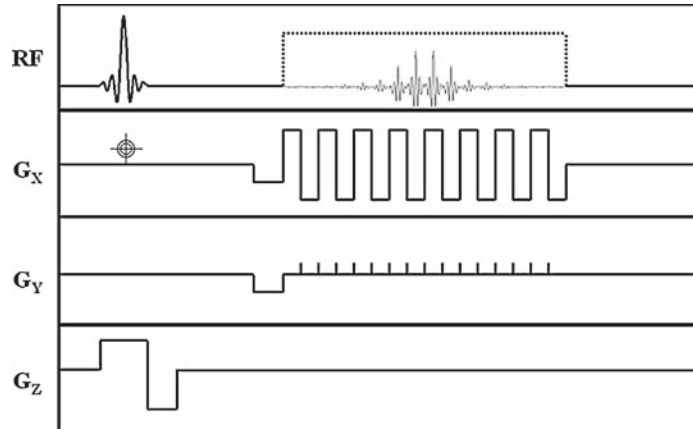


Fig. 9. Blipped echo-planar imaging (EPI) pulse sequence. Readout gradients are reversed following readout of each k_x line, along with a small increment of k -space in k_y direction, or a “blip” in G_y . Sixteen k_y lines are read out, corresponding to the k -space diagram in **Fig. 7**. Gradient-stimulated echo train is shown in *light gray*, which becomes stronger closer to center of k -space, and at center of each k_x -readout.

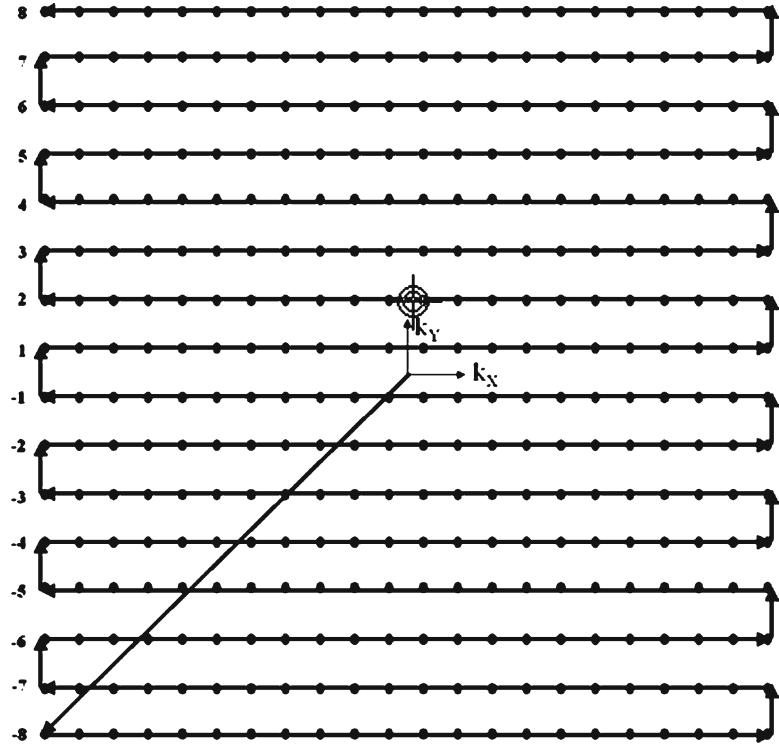


Fig. 10. Cartesian trajectory in k -space for one-shot blipped echo-planar imaging (EPI) sequence shown in **Fig. 5**. One-shot means full coverage of k -space is accomplished during echo of one excitation.

manner, such as in **Fig. 11**, with less asymmetry between the rate of sampling in k_x - and k_y -space.

By applying sinusoidal gradients 90° out of phase to the read- and phase-encode gradients, k -space can be traversed in a circular manner by increasing the amplitude of the sinusoidal gradients. A typical sequence for spiral acquisitions is shown in **Fig. 12**.

This process continues until k -space is adequately sampled. There are many trajectory modifications to this scheme, but all have the basic property that the sampling of k -space is not Cartesian, but instead approximately radial symmetric. Reconstruction of image space from k -space may be done using a Fourier transform after resampling the k -space data to a Cartesian grid, but there are implementations that reconstruct the image data using the discrete Fourier transform (10, 11).

Spiral imaging has advantages compared with blipped EPI, mostly related to the lower overall demand on the gradients. These include reduced gradient noise, improved SNR, lower induced eddy currents,⁴ and different geometric distortion artifacts (12).

⁴Eddy currents are currents induced in gradient coils and other scanner components from the rapidly changing fields generated by the gradient coils.

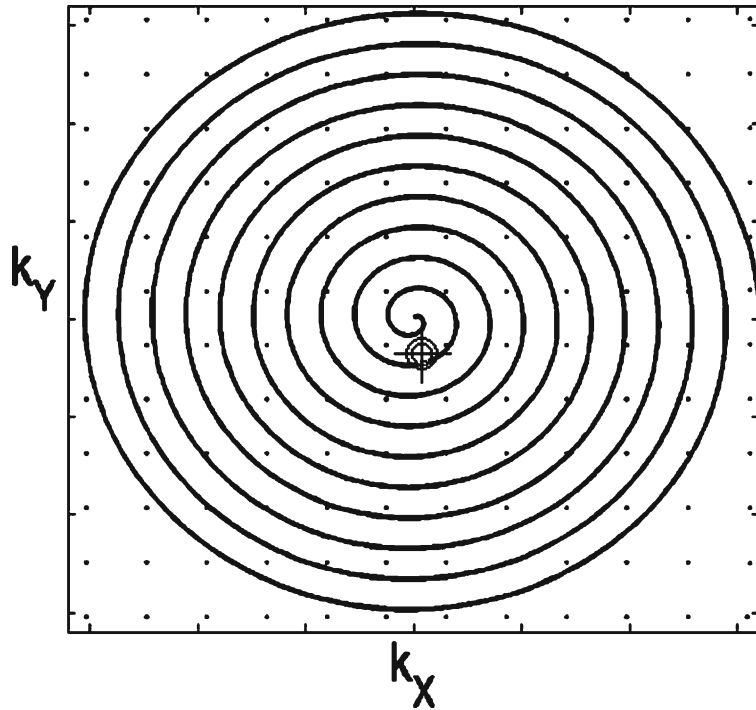


Fig. 11. k -Space sampling trajectory for a one-shot spiral imaging sequence shown over a rectangular grid. Central k -space is sampled first. Prior to fast Fourier transform (FFT) reconstruction, the data must be resampled from spiral grid to Cartesian grid.

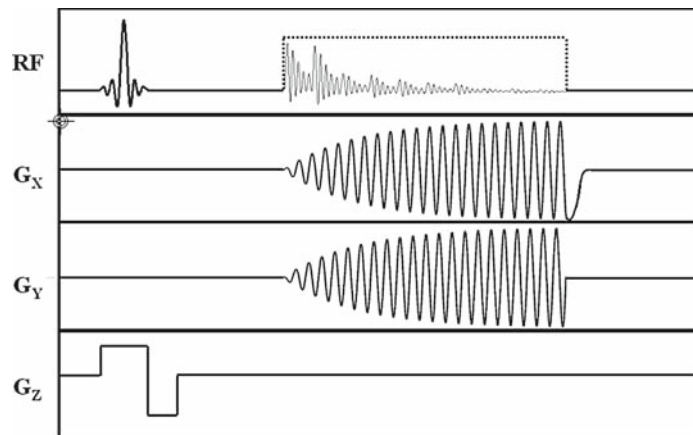


Fig. 12. Pulse sequence timing diagram for spiral acquisition. Gradients during readout window are 90° phase-offset ramped sinusoids.

Increased SNR is due to the earlier sampling of the center of k -space, but the correspondingly later acquisition of the outer regions of k -space mean that the higher spatial frequencies have lower specificity than the readout direction of a blipped-EPI

image. The typically sinusoidal gradient play-out means the gradients are switched at a lower rate of change, which reduces the induced eddy currents and gradient noise. Since most of the magnetization signal naturally lies near the center of k -space, which is sampled early, it is preferable to start the readout window at the TE. This modifies the timing from the Cartesian EPI sequence where the readout is centered on the TE, although newer spiral sequences (such as spiral-in/out) are available which also center the TE in the readout window (13). A spiral-in/out sequence is shown in Fig. 13.

A spiral-in/out sequence reduces the effects of the echo shifting by centering the readout at the TE as in EPI. Readout begins prior to the TE, starting near the edges of k -space and spiraling into the center, which is reached at the TE, before spiraling back out over new data points. After resampling the grid, every point in k -space now has two samplings symmetrically spaced about the TE, which are passed through FFT to give two images. These two images can be combined and the result is a reduced sensitivity to susceptibility signal loss and image data with an effective TE closer to that specified (14). This is more demanding on the gradient hardware than spiral imaging and there can be drawbacks in image quality.

2.4. Parallel Imaging

Multiple receive coils have become a popular and widely available means to increase image SNR by providing multiple samples of a k -space trajectory. Because the coils cannot be located in the same place, they have varying spatial sensitivities to the tissue, which is maximal at the tissue nearest each coil element. This provides an alternative spatial encoding mechanism, where

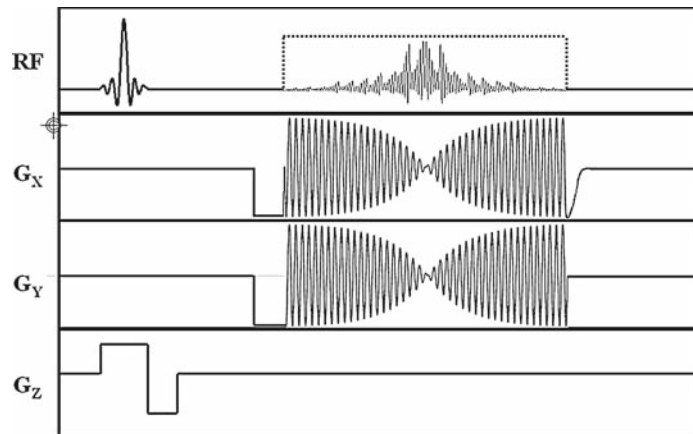


Fig. 13. Spiral-in/out sequence acquires full k -space data prior to echo time and a second acquisition of k -space after echo time. The data from these echoes are combined in reconstruction.

one sample of several parallel coil elements provides information about the magnetization density over several regions of tissue. Parallel imaging combines this spatial encoding with the gradient-mediated spatial encoding to skip some gradient-encoded lines in k -space and replace those gaps with information derived from the parallel coil elements (15). The skipped lines in k -space reduce the field of view (FOV) seen by the coils by a reduction factor. The individual coils, if reconstructed with only the data acquired, would see the nearest portion of tissue inside that coil's FOV, but with aliased image overlap with other portions of tissue further away from the coil. The methods used to un-alias the data can be separated into two strategies: image-space unfolding and k -space interpolation. While there are many methods, and more than a few hybrids, the most common implementations of each [sensitivity encoding, SENSE (16), and generalized autocalibrating partially parallel acquisitions, GRAPPA (17)] will be discussed, along with benefits/drawbacks.

2.4.1. SENSE

SENSE performs the reconstruction of parallel images in image space in an iterative manner using a seeded coil sensitivity matrix. Prior to the parallelized scan, the sensitivity of each coil in the full FOV is measured. These sensitivity maps are used as an initial guess for the “unfolding” matrix.

The undersampling of k -space shown in **Fig. 14** leads to image aliasing when reconstructed. However, if the multiple coils are sensitive to spins from different aliased regions, then the portion of signal aliased or unaliased in each image can be differentiated using the sensitivity of the multiple coils to the different regions. The matrix inversion is performed iteratively after preprocessing the data to handle the problem of nonideal coil geometry.

2.4.2. GRAPPA

GRAPPA is a regenerative k -space method, using measured data to calculate missing phase-encoding lines. Outer regions of k -space have reduced sampling. The acceleration factor defines the number of lines skipped per line acquired. The central k -space lines, or autocalibration signal (ACS) lines, are fully sampled, which is shown in **Fig. 15**.

The ACS lines are used to interpolate the nonacquired lines of k -space by fitting the acquired lines to the ACS data. This is performed separately for each coil used, leading to weights specific to each ACS line, for each coil. So for N coils, there will be N^2 weights resulting from the fitting procedure to use in interpolating the nonacquired lines. A particular coil's matrix is based on all coil signals, but masks out, or de-weights, signal from other regions outside the FOV of that coil, in k -space. The matrix weighting removes the aliasing seen in the original, under-sampled images. The final, unaliased image data for each coil is combined by sum-of-square. The greatest advantage of GRAPPA

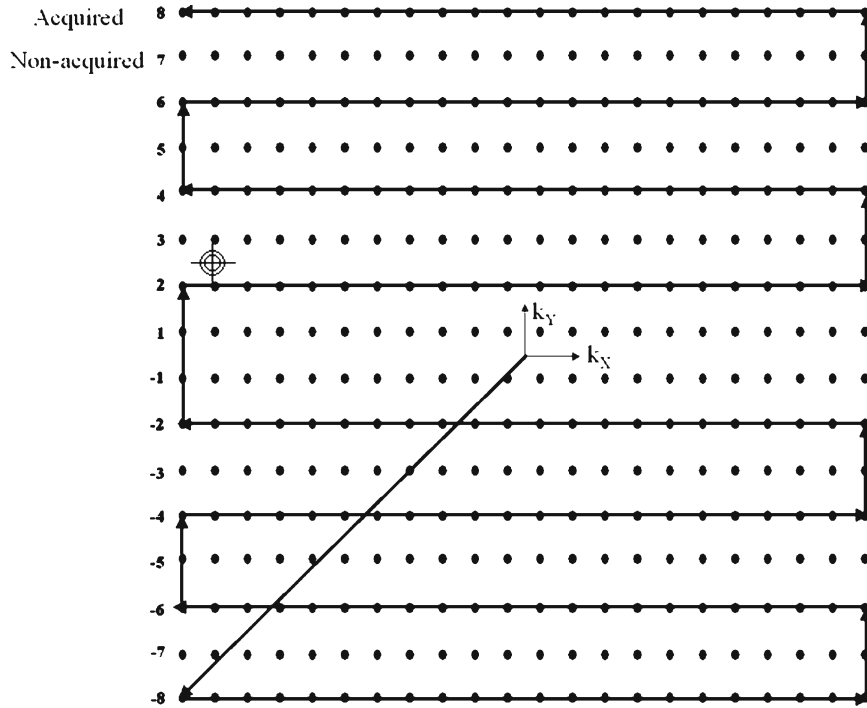


Fig. 14. Sensitivity encoding (SENSE) k -space traversal for acceleration factor 2. Odd lines of k -space are missed, even lines acquired. Acceleration factor equals acquired plus nonacquired number of lines, divided by acquired lines, in this case the full k -space matrix would have twice the number of lines as were actually acquired.

over image-space methods is the determination of sensitivity from the k -space data itself, which is useful in images containing regions with poor homogeneity or low signal, both of which are the case with ultrafast imaging (18).

2.4.3. Tradeoffs

The primary benefit of parallel imaging is a reduction of the time spent spatially encoding (the readout window), but at a cost of SNR compared to the same sequence with a fully gradient-based spatially encoded image using the average signal from the parallel coils (19, 20). The reduction in SNR is due to reduced coverage of k -space, or the square root of the acceleration factor. An additional cost for any parallel imaging is the coil geometry coverage or g -factor. In SENSE imaging, the g -factor directly relates to the invertibility of the sensitivity matrix (21). Since most ultrafast parallel blipped-EPI sequences are acquired in two dimension only, the coil coverage should be optimized in the phase encoding direction (22). Spiral-EPI with parallel imaging is more complicated than blipped-EPI and much more time consuming but recent advances have reduced the reconstruction time for parallel spiral-EPI (23–25).

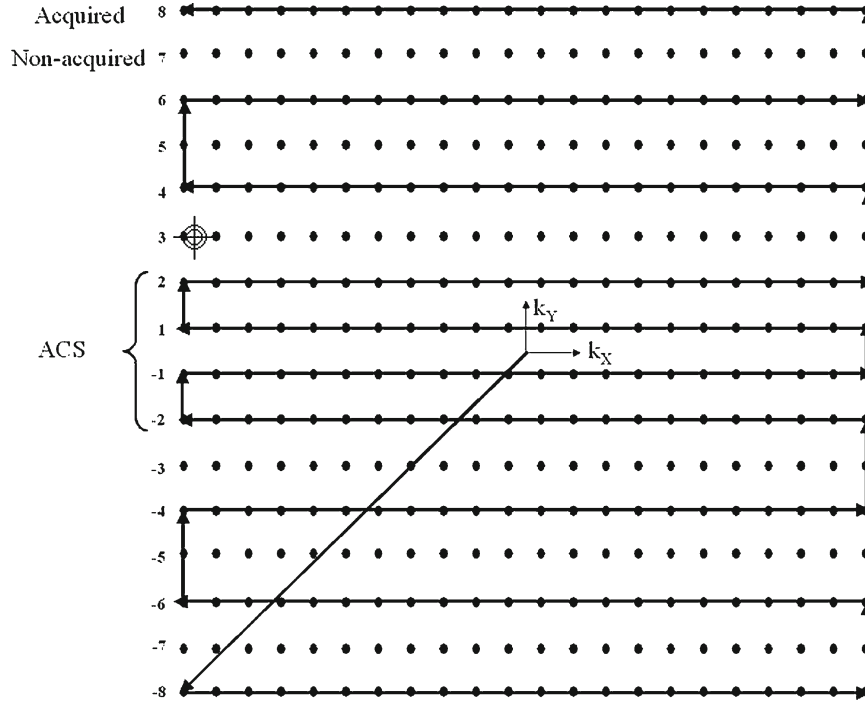


Fig. 15. Generalized autocalibrating partially parallel acquisitions (GRAPPA) k -space traversal. Central k -space is fully sampled to provide ACS lines. Outer k -space is undersampled in phase-encoding direction by acceleration factor. Acceleration factor here is 2, so every other line is acquired. Same sampling is acquired for other coils.

2.4.4. Artifacts

Residual alias in the image is a common artifact seen with parallel imaging. The SENSE method requires the full image FOV to be greater than the object of interest in any accelerated directions; otherwise reconstruction will fail resulting in considerably aliased images. The only current solution with SENSE is to expand the FOV so that there is no image wrapping (26). This is not an issue with GRAPPA, because the spacing of k -space lines determines the FOV, but not the signal of a particular line. Therefore, k -space fitting under GRAPPA is not compromised by a smaller FOV, while image space fitting would be compromised by the aliasing image. With an ideal sensitivity map, SENSE gives better results than GRAPPA, however, the accuracy of the maps are highly dependent on local field homogeneity and subject motion can invalidate them. There are now several sensitivity map methods, including ones based in part on GRAPPA autocalibrating methods that derive the maps from the data to get around these problems (27). Finally, there is the issue of fitting the systems of equations in the presence of incomplete coil coverage. The SENSE method requires the solution of an inverse problem, but

if there are regions of tissue that no coil has adequate sensitivity to, this is an ill-conditioned problem that cannot be exactly solved. All implementations of SENSE regularize or condition the data to work around this, but it means that the final reconstructed image may have local noise enhancements (28–30). GRAPPA is also sensitive to this problem, but because fitting is done with k -space data, the noise enhancement is global rather than local (21).

2.4.5. Limitations

There is a practical limit to the number of coils and the acceleration factor, because adjacent coils will overlap spatially in their sensitivity and coverage of magnetized spins, reducing the ability to separate aliased signals. In typical applications of ultrafast imaging, the use of two-dimensional EPI sequences leads to a limit on the acceleration factor of between 4 and 5 (19). While not every scanner has multiple channels, it is becoming the standard for vendors to offer such capability. However, most sites are unable to use parallel imaging due to higher than expected SNR loss at even the lowest acceleration factor (31). Future implementations of parallel imaging promise higher acceleration factors with less loss of SNR using hybrids of k -space and image-space methods with dynamically changing undersampling strategies, such as k - t SENSE (32) or k - t GRAPPA (33).

2.5. Partial Fourier Imaging

Ideal k -space data has complex conjugate symmetry, which can be exploited to reduce the acquisition time. Up to half of k -space can be interpolated from symmetry with the other half. This is referred to as partial Fourier imaging. The symmetry is only approximately true in real data due to scanner and tissue nonidealities, so algorithms to take advantage of this fact must use low-resolution approximations to account for nonzero phases in regions breaking this symmetry (34, 35). With the use of partial Fourier acquisition, a higher spatial resolution can be acquired with less signal loss and blurring, with the result that the SNR does not drop along with the reduced acquisition time (36, 37).

3. Artifacts

3.1. Nonphysiologic

There are several potential artifacts from single-shot imaging techniques due to hardware realities, such as chemical shift (fat) artifact, eddy current artifacts induced by the fast gradient switching, imperfections in gradient ramping waveforms, and both blurring and signal loss due to nonuniform TEs combined with static-field inhomogeneity.

3.1.1. Water-Fat Shift

Water-fat shift image artifact is a consequence of the off-resonance frequency of body fat that shifts the fat signal mostly in the phase-encode direction, misplacing it across the image. Fat suppression with an RF pulse at the resonance frequency of fat, often called chemical saturation, followed by a strong dephasing gradient is the standard countermeasure on EPI sequences. This RF pulse is done immediately before the initial excitation pulse and, due to the fact that the longitudinal signal of the fat is saturated, water protons in fat will experience no excitation. One immediate consequence of this approach is an increase in the time taken by the sequence, as this off-resonance pulse must be performed once before every excitation pulse. Because the resonance frequency of fat protons is only 3.35 parts per million (ppm) in frequency away from water protons, the homogeneity of the static field must be very good to help ensure that the suppression pulse acts only on fat protons and the excitation pulse acts only on water protons.

An alternative strategy to chemical saturation is the use of spatial-spectral RF excitation pulses (38). These are patterned RF and gradient pulses played out over many milliseconds. Properly designed, the aggregate affect of the ensemble of pulses is to create discrete regions of excitation in space and frequency. It is possible to design these pulses such that the excited regions are separated by more than 3.35 ppm in frequency, such that water protons in tissue in a given slice will be excited and water protons in fat will not. This strategy requires less field homogeneity than chemical saturation, but they tend to have a poor slice profile and can take up to twice as long as a good chemical saturation pulse to achieve the same result.

3.1.2. Gradient Nonidealities

Time-varying magnetic gradients induce eddy currents in nearby electrical conductors, such as the magnet cryostat. These eddy currents create magnetic fields that partially cancel the effect of the applied gradients. Fast gradient ramping is limited in hardware by the reactance of the gradient coils, creating effective upper limits on gradient switching that perturb the intended ramping waveform that the gradient coil is driven with. These waveform perturbations increase as gradient switching time decreases. The induced eddy currents and gradient ramping imperfections create phase errors in k -space magnetization readout, which produces different artifacts depending on the k -space trajectory.

In blipped-EPI, artifact is magnified in the phase-encode direction. This creates what is known as a “phase ghost” or “N/2 ghost,” an identical image at 2–5% of the original image signal level but offset by 90° in the phase-encode direction. The ghost can have some overlap with the image of interest. In spiral EPI, the artifact is not as simple, but will result in an increase in noise level.

The corrective methods used vary by scanner manufacturer, but there are some commonalities. The first line of defense is in the screening of the gradient coils to reduce the field change and concomitant eddy currents. A second method employed is calibration of the gradient waveforms. To an extent, eddy currents can be predicted and compensated for by pre-emphasis of the gradient waveforms. This is shown in **Fig. 16**.

Generally, the effect of coil reactance is to dampen the intended gradient waveform by providing a resistance to it, so the waveform to be played out on each gradient coil is modified by a predetermined calibration. Changing the configuration of conductive objects in the scanner room can make this calibration obsolete, if they are near and large enough to be affected by the gradient fields. This could show up as a sudden increase in $N/2$ ghosting in blipped-EPI images, requiring a recalibration of the gradient waveform perturbation. Further antighost calibrations to account for system timing offsets and residual eddy current effects may be performed, such as phase line correction. A calibration is typically taken just prior to the readout window in the blipped-EPI sequence by sampling forward and backward across the middle of k -space. Eddy current and timing offsets result in a nonideal k -space trajectory that can be approximated as a simple shifting of each line of k -space forward and backward depending on the direction of traversal. The calibration lines are used to resample every readout k_y line to center the received echo (39, 40). A failure of this online phase ghost correction algorithm would show up as a dramatic increase in phase ghost signal level, to a level comparable to the image of interest. An example of a failure of online phase ghost correction is shown in **Fig. 17**. In this case, signal changes seen as a result of phase ghost correction overwhelm the BOLD effect.

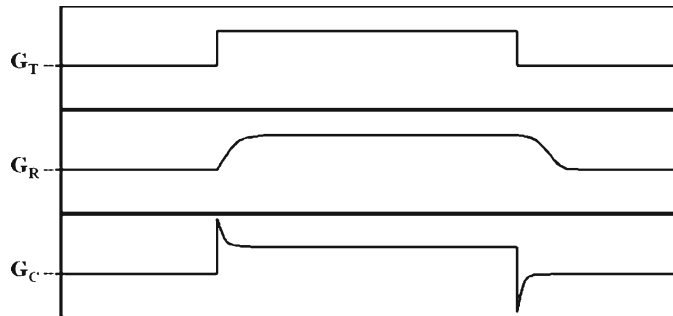


Fig. 16. Gradient waveform calibration. G_T shows the theoretical, intended gradient, while G_R shows the real waveform due to eddy current damping the intended waveform. G_C shows a calibrated waveform to be played out on the gradient coils to produce the intended gradient despite the presence of eddy current.

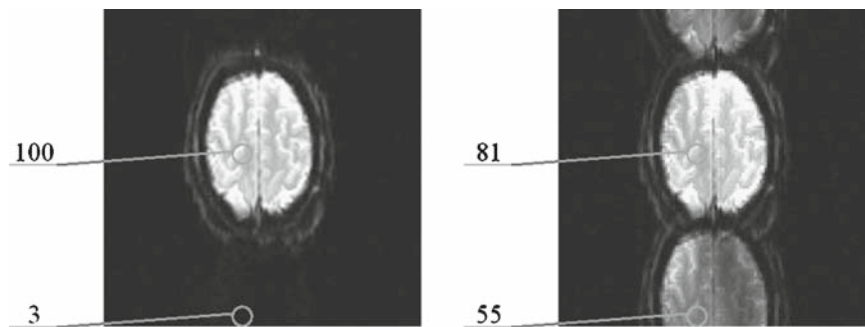


Fig. 17. Phase ghost typical level on *left*. Phase ghost correction algorithm failure on *right*. All measured signal values normalized to first brain tissue measurement on *top left*.

The effect of eddy current on spiral imaging is smaller since dB/dt is lower, but if uncompensated will result in warping, because it warps the k -space trajectory in both dimensions. Measuring the actual trajectory taken in k -space can be used in the resampling portion of reconstruction to correct this image warping similar to the blipped-EPI phase line correction (41).

3.1.3. Echo Shifting

The long readout time employed leaves single-shot images highly sensitive to static field homogeneity, leading to image distortion artifact in regions of inhomogeneity. The off-resonance frequency in these regions causes an accumulation of phase errors in those regions over the readout time. Phase errors specific to a region result in spatial encoding errors, which manifest as signal misplacement from that region. For blipped-EPI images, this is insignificant in the readout, or k_x direction because it is sampled so quickly, but the phase-encode direction is sampled more slowly, resulting in spatial distortion, or blurring in the phase-encode direction in those regions. Spiral imaging samples the k_x and k_y dimensions at approximately the same rate, but the radial dimension is sampled more slowly, akin to the phase-encode direction in EPI. Spiral images are therefore blurred across both dimensions (42). The geometric distortion can be “unwarped” from the images using the calculated pixel shifts from an acquired fieldmap for both blipped-EPI (7, 43) and spiral imaging (35) (Fig. 18).

3.1.4. Signal Loss

Signal loss, or slice dropout, is caused by through-slice dephasing after the RF excitation. This signal loss cannot be recovered without modifying the pulse sequence. Strategies for overcoming this include: use of SE to refocus the dephasing effects, reducing the TE, reducing slice thickness and/or in-plane voxel size, and changing the scan plane. If hardware permits, the use

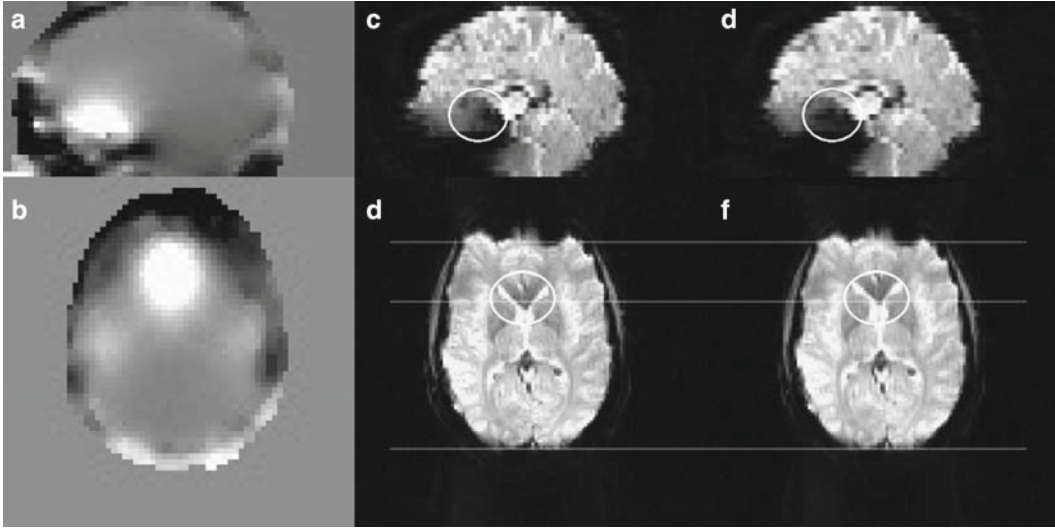


Fig. 18. (a) Sagittal, (b) axial views of fieldmap. Other pictures show (c) and (d) blurred blipped echo-planar imaging (EPI) signal and (e) and (f) unwrapped images of the same using pixelshifts calculated from the fieldmap. Anterior regions shifted roughly 1–2 pixels, but signal loss near the frontal sinuses cannot be recovered, leaving a signal void.

of high order gradient shims and image-based shimming can help (44–46).

Another common method is z -shimming to unwrap some of the dephasing, but this has the disadvantage of reducing the SNR in unaffected regions. z -Shim methods rely on acquiring a fieldmap to estimate the gradient across a slice, and then applying an opposing (negative) slice gradient that is equal to the fieldmap measured gradient in the high susceptibility region (47, 48). This reduces the dephasing in the high susceptibility region, but at the cost of increasing dephasing in other less-affected regions. To deal with this problem, typically two images are taken; one with the z -shim and one without and then these are added together to restore all signal loss, but at the cost of nearly doubled imaging time. This method is approximately equivalent to an older technique of tailoring RF pulses to apply a set dephase across the slice at the time of excitation (49). Alternatively, several images with a range of z -shim gradients linearly spaced between zero and the maximum measured gradient are taken, and these are averaged; however, this is more time consuming with little benefit over the more common method with two images.

3.1.5. Spiral Regridding

Apart from lower spatial specificity and increased acquisition time, problems typically associated with spiral imaging lie in the regridding of the spiral trajectory to a Cartesian coordinate system prior to Fourier transform. Regridding introduces subtle

artifacts and reduces SNR, and is computationally intensive compared with the reconstruction methods used in blipped EPI, although computational improvements have been made (50, 51). Until recently, the reconstruction had to be performed offline on a separate image-processing computer after the scan, which made it difficult to validate data online or use prospective motion correction. There are now online versions of spiral reconstruction, such that prospective motion implementations for spiral imaging have been used to monitor subject motion (52).

3.2. Physiologic Artifacts

There is another class of image artifacts present in functional neuroimaging that have physiologic origins. Head motion (53–55) and physiologic noise from the heart and breathing cycles (56–58) are unavoidable nonneuronal sources of variance, changing underlying statistical distributions and introducing possible systematic effects in population studies. Accounting for these artifacts requires care in the acquisition of data and several stages of postprocessing of data (retrospective techniques will not be discussed here) after collection is complete. Preventive measures include head restraints or navigator echoes to reduce the effects of head motion, and routine scanner quality assurance measures to track the stability of the scanning hardware (59). In addition, the collection of parallel measures of state during the image acquisition may be useful for artifact removal during postprocessing. These parallel measurements can include online motion detection parameters from navigator echo or prospective motion correction along with signals representing physiologic cardiac and respiratory cycles.

3.2.1. Head Motion

Due to the fact that it is desired to maintain a high temporal resolution, the sampling rate in most fMRI acquisitions is fast compared to the T_1 of brain tissue. The consequence of this is that, after equilibrium is achieved after acquisition of a few volumes, the tissue is in a saturated state. This means that the magnetization is not completely recovered between excitations of a given slice. If a subject moves such that tissue from one slice moves into an adjacent slice, the tissue will, for the first excitation after the motion, be in a different state of saturation than the rest of the tissue in that slice. This leads to a signal change that is correlated with the motion, but will not be corrected by the traditional technique of retrospective realignment of the images. Prospective motion correction techniques are intended to deal with this problem in real-time.

Navigator echoes can be used to obtain motion information during the acquisition of data (60, 61). This technique uses the fact that the phase of MR data is sensitive to motion. Typically, low-power RF pulses are interspersed with the fMRI data acquisition and the phase information from the readout of the signal

from these pulses is used to infer motion along a given direction. The drawbacks of the navigator echo approach is that, unless the power is very low, in which there is a limited ability to determine phase changes, the excitation pulses will affect the spin history of the fMRI data. Nevertheless, these approaches have been used with some success in fMRI.

An alternative approach that has been applied is to use real-time coregistration of a reference volume to the current volume to determine motion. The motion parameters are determined from the coregistration and are applied to the imaging system prior to acquiring the next volume (52, 62). The drawback of this approach is that it is more computationally intensive than the navigator echo approach and it does not update the slice locations until after the motion occurs. Thus, registration-based prospective motion correction must be coupled with postprocessing motion correction.

3.2.2. Physiologic Noise

Ongoing physiologic processes in living subjects present an additional potential artifact. Effects due to the cardiac and respiratory cycles have been identified as being significantly coupled to BOLD-weighted MR signal in voxels in the brain and the spinal cord. The primary effect of the respiratory cycle on blipped-EPI fMRI data is an apparent shift in image position in the phase-encode direction. This is due to shifting of the resonant water frequency as the main field drifts due to chest expansion and contraction (63, 64). The primary effect of the cardiac cycle is pulsatility artifact with each heartbeat, although the structure and timing of the artifact may vary across the brain due to the range of vessel sizes, stage in the vessel network, and location in the brain (65, 66). The cardiac effects are more pronounced in certain regions such as the insula and brainstem, while respiratory effects are more global (Fig. 19).

Correcting for the effect of respiration can be accomplished using navigator echoes or off-resonance detection to follow the field shift during the scan, in the same way as described above for gross head motion. Gating acquisitions on either cardiac or respiratory rates is another method that has been used to reduce the variability in fMRI data (67). This approach necessitates a correction for T_1 effects introduced by the variable TR.

Use of parallel measures can be used to effectively remove physiologic noise sufficient for most purposes in fMRI (68, 69). Therefore, acquiring a pair of signals representing the cardiac cycle and respiratory cycle during the scan is desirable, although recent methods have been developed to estimate equivalent signals from the echo-planar data itself (70).

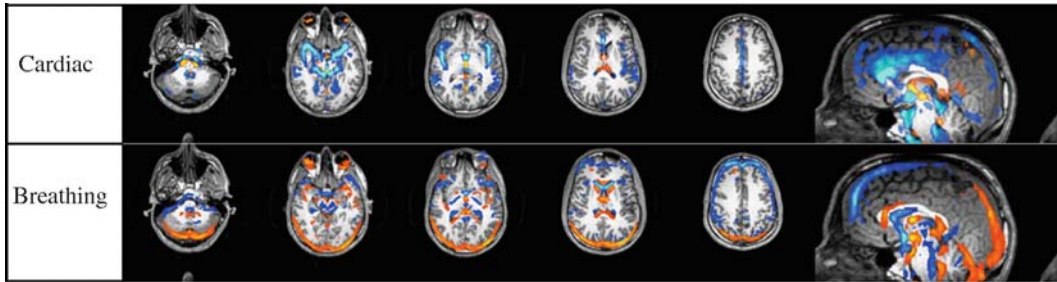


Fig. 19. Averaged physiologic coupling maps in blipped echo-planar imaging (EPI) with phase-encode direction in anterior-posterior axis, determined by temporal independent component analysis (ICA). Cardiac coupling overlain on anatomy is shown in *top row* and respiratory coupling is shown in *bottom row*.

4. Optimization of Sequence Parameters

In order to generate MRI data with functional contrast, there are a number of experimental issues that need to be considered. Generally speaking, if the issues were simply rapidly generating images with BOLD contrast then the procedure would be to simply select sequence parameters such that the TR is as short as possible and the TE such that the expected changes in capillary or venous oxygenation result in a maximal signal change between rest and active neuronal state. However, the choice of optimal acquisition encompasses many other experimental issues and these should all be considered.

4.1. Relaxation Parameters and Functional Contrast

As described above, BOLD contrast in MRI is produced either through changes in T_2 or T_2^* . We are interested in optimizing MR signal differences between two states, rest and active. In this section, we discuss scanner and sequence issues that can affect the detection of these two states.

4.1.1. Field Strength and Relaxation Parameters

The effect of static field strength on T_2 relaxation in brain tissue, as evidenced from examination of **Table 1**, is generally that it is reduced. The effect of field strength on the BOLD signal is complex, and depends on the nature of the proton transport mechanism in the presence of the field defects introduced by the deoxygenated hemoglobin. Recent studies suggest that this mechanism is largely diffusive in nature at clinical field strengths, which would suggest a linear dependence of the BOLD signal on field strength. Experimental data bear out the linearity of the dependence of BOLD contrast on field strength (71). Thus, BOLD contrast from extravascular protons can be taken to increase approximately linearly in the regime used by most commonly available MRI scanners (i.e., 0.3–3.0 T).

The intravascular contribution to BOLD signal stems from the impact of the change in oxygenated hemoglobin concentration within the vessels and the consequent change in T_2 of the blood. The effect of this at the voxel level has been more difficult to describe than the extravascular effect due to the dependence on many factors such as blood volume, vessel size, and volume fraction.

4.2. Experimental Design

The goal in experimental design of fMRI studies is to take advantage of the fact that regional changes in blood flow and oxygenation result proximal to regions of increased neuronal activation. Historically, the basic methodology has been to acquire properly weighted MRI data of the brain regions of interest while a subject repeatedly performs tasks related to the brain function of interest. Initial methodology took advantage of the observation that continuously repeating a task during short intervals leads to an accumulation of signal from the overlapping of events in a time short compared to the hemodynamic response. This is a feature of the general linear model (GLM) of functional imaging (72).

Blocking activation in bursts of extended activity over many seconds, interleaved with long period of rest, leads to up to a much higher increase in hemodynamic response than short, isolated events. This fact makes it desirable, when possible, to use what is typically referred to as a *block design*.

In 1997, Josephs and colleagues proposed an alternative experimental design, intended to more specifically detect the MRI signal associated with neuronal events (73). This experimental design takes advantage of the fact that, through synchronization of the time of stimuli and measurement of behavioral responses, functional imaging data can be analyzed for signal fluctuations correlated with brief, temporally separated neuronal events. This type of experimental design is referred to as *event-related fMRI*. Due to its suitability to address more complex neuroscience questions regarding brain activation and interactions, this has become a preferred experimental design among neuroscience researchers.

Since these two experimental approaches have different analysis strategies, the issues with regard to optimizing pulse sequences are different between them. In the sections below, we separately discuss these issues.

4.2.1. Block Design fMRI

As stated above, block design fMRI experiments are designed to create a large aggregate signal from activated neurons extended in time, interspersed with long periods of rest, or alternate task performance. Analysis of this type of data is typically performed with what is referred to as a reference function. The simplest method for analyzing these data is simply to calculate the cross correlation of the experimental reference function with the time series at each voxel (74). Although more sophisticated methods

have been developed that allow more complex analyses, accounting for nuisance effects and systematic effects of no interest, for purposes of pulse sequence optimization, a correlation approach is sufficient to illustrate the issues.

Figure 20 shows an example of the signal time course from a voxel in response to a block design paradigm. The issues with regard to pulse sequence optimization are contrast-to-noise ratio (CNR), sampling rate, and number of samples. In principle, the TE and TR will control the CNR for a given pulse sequence (i.e., EPI, spiral, etc.). The sampling rate is the inverse of the TR. The detection efficiency of a pulse sequence will be determined by these and the number of samples. As an illustration of this, **Fig. 21** shows the probability of getting a type II error at a false positive rate of 0.01 as a function of the number of samples.

4.2.2. Event-Related fMRI

Event-related fMRI relies on a different analysis strategy than block design fMRI. The principal difference as it relates to choice of pulse sequence is temporal resolution. A typical method for analyzing event-related fMRI is *deconvolution*. Deconvolution is an analysis method where rapidly repeated, although temporally separated, events can be extracted if the timing of the onset of the signal and either the duration or the hemodynamic response function is known. A detailed discussion of deconvolution techniques is beyond the scope of this chapter. The reader is referred to chapter 7 for a more complete treatment of the analysis of event-related fMRI.

Figure 22 shows a typical timing and signal response for a rapidly presented event-related fMRI experiment. Studies on the

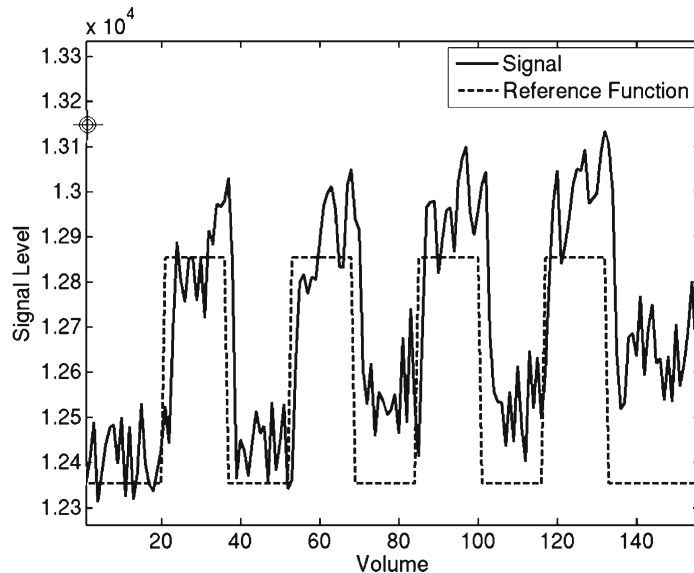


Fig. 20. Example of fMRI timecourse from a voxel for a block-design experiment.

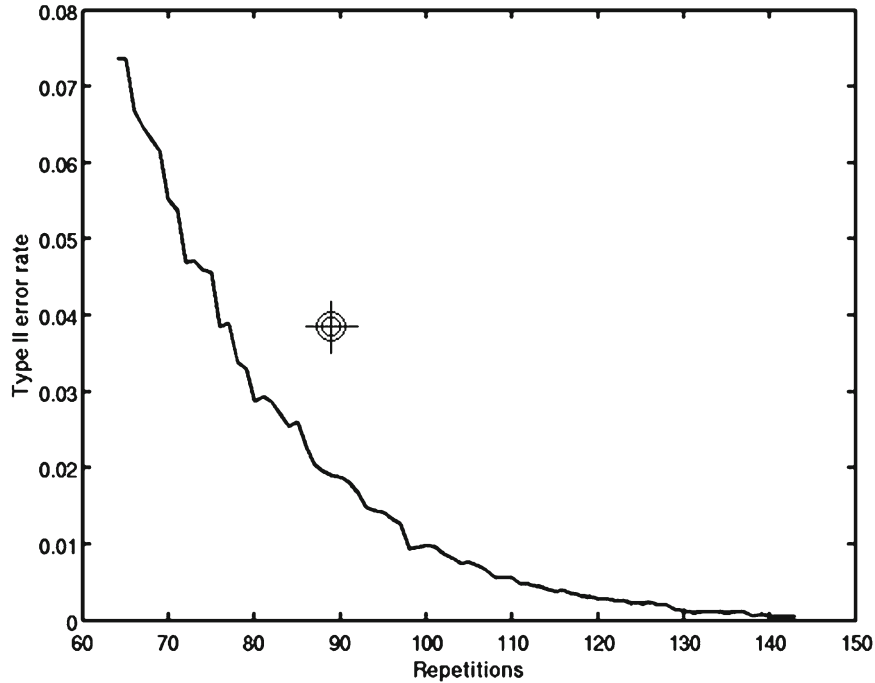


Fig. 21. Probability of rejecting a true event (type II error) as a function of the number of samples at false positive rate of 0.01 for a two cycle block design fMRI experiment. Result is from simulating image (signal-to-noise ratio = 50 with a 2% blood oxygen level-dependent signal change).

ability of deconvolution techniques to resolve neuronal timing shifts indicate that volume sampling rates (i.e., TR) of up to 3 s permit identification of neuronal timing shifts of order 100 ms (75). Therefore, if a goal of an experiment is to study relative timing of events, TRs of up to 3 s should be sufficient.

Another pulse sequence issue that should be of concern to researchers employing event-related experimental designs is SNR. As stated above, the CNR of event-related design is much lower than block design experiments. Therefore, it is recommended that researchers choose their acquisition strategy with this in mind. For instance, if a local cortical region is of interest, a surface coil array could be adopted to significantly increase SNR. Pulse sequence choices should be made carefully to avoid loss of SNR (shortest TE permissible for BOLD contrast, for example). In **Section 5**, issues with regard to SNR for the common pulse sequence parameters will be discussed in detail.

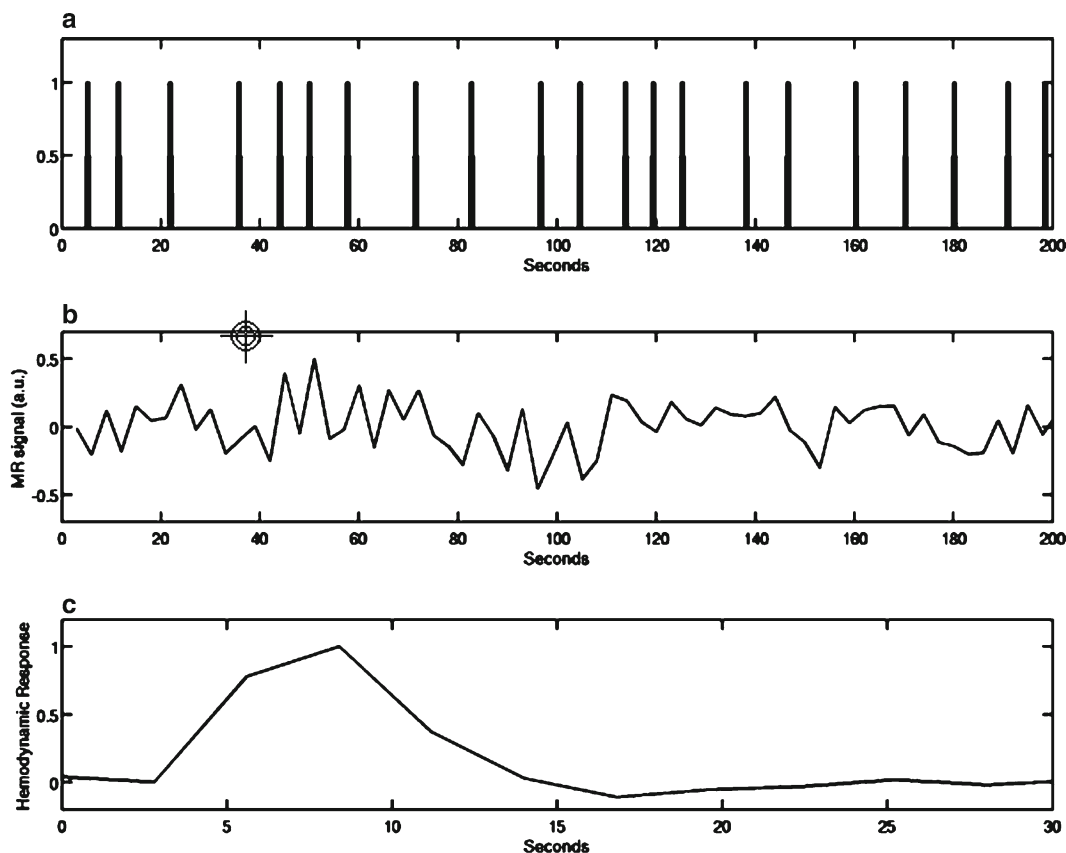


Fig. 22. Example of event-related fMRI experiment. Rapid presented stimuli (a) results in single-voxel time series shown in (b). Hemodynamic response (c) is deconvolved from signal average over 100 voxels with temporal resolution 3 s.

5. Summary Recommendations for Optimal BOLD fMRI

In this section, we will summarize the issues with regard to pulse sequence optimization in the performance of fMRI experiments. As stated above, currently, BOLD-weighted fMRI is the overwhelming method chosen for fMRI. For that reason, the recommendations presented in this summary will focus on BOLD-weighted acquisitions. In most cases, the technical discussions will be relevant for other types of image weighting.

In the context of the information presented previously in this chapter, we will present recommended acquisition strategies for a given field strength and we will then expand on the optimization issues with regard to each of the sequence parameters.

Table 2 lists basic pulse sequence recommendations for two field strengths and two experimental design strategies.

Table 2
Basic sequence parameters for BOLD fMRI acquisition on most clinical MRI scanners

Sequence parameter	Field strength	
	1.5 (T)	3.0 (T)
Sequence	GRE-EPI	GRE-EPI
Scan plane	Axial	Axial
FOV (mm)	256 × 256	256 × 256
Matrix	64 × 64	128 × 128
TE (ms)	50	30
TR (ms)	2,000	2,800
Flip angle	77°	80°
Receiver bandwidth (total) (kHz)	125	250
Slice thickness (mm)	7	4
Slices (for whole-brain coverage)	18	32

FOV Field of view, *GRE-EPI*, gradient recalled echo–echo planar imaging, *TE* echo time, *TR* repetition time

The recommendations in **Table 2** should be possible in almost any recently installed clinical MR scanner of the indicated field strength. Further recommendations made below may require special modifications to supplied clinical pulse sequences and it is strongly recommended that researchers seek the input of an MRI physicist experienced in fMRI.

5.1. Pulse Sequence

Various pulse sequences that have been proposed for fMRI acquisition were outlined in **Section 2**. Issues with regard to optimization of fMRI experiments are discussed here.

5.1.1. Echo-planar Imaging

This is now the most commonly available single-shot imaging sequence available on MRI scanners. Data can be acquired in GRE mode and SE mode.⁵ The issues with regard to optimization

⁵In addition, a mixed mode EPI has been used in the literature known as asymmetric spin echo (ASE). This is a SE EPI with the acquisition window shifted to be centered on a time point early on in the SE evolution. The result is an acquisition that has, in a sense, *adjustable* sensitivity to capillary and venous signal.

are that SE EPI employs, by necessity, a longer TE that will result in a smaller intravascular contribution, particularly at 3.0 T and higher, and refocuses dephasing effects from the static dephasing component of the extravascular signal that is specific to larger, distal vessels. The result is that SE EPI can be more spatially specific to the localization of neuronal activation. However, the SNR is much lower than GRE EPI. SE EPI is not recommended for field strengths below 3.0 T because the T_2 of blood is not short enough to be of benefit with regard to the intravascular BOLD signal and the SNR is too low to employ high enough spatial resolution for the spatial specificity to have a significant impact.

5.1.2. *Spiral Imaging*

Spiral imaging is becoming more common and is available as a product sequence on some clinical MRI scanners. As outlined above, the major advantage of spiral imaging with respect to EPI is that it is less demanding on the imaging gradients. Thus, there will be reduced image warping from eddy current effects. In addition, the nonuniform sampling of the Fourier domain image will lead to a different, possibly lower, sensitivity to motion effects and even some types of physiologic noise. Variants of the spiral technique have been proposed that are specifically designed to be more sensitive to the characteristics of the BOLD signal. This sequence is recommended for researchers employing systems with underpowered gradient systems and for situations where motion and/or physiologic noise or other types of image artifact, as discussed above, are a concern and alternate methods of addressing these are not available.

5.1.3. *Parallel Imaging*

MRI scanner manufacturers are increasingly moving to the use of head array RF coils in lieu of circularly polarized quadrature head RF coils for MRI. The cost, particularly at 1.5 T, is uniformity of SNR, and thus fMRI signal detection efficiency across the brain. This is less of an issue at high field strength, since dielectric effects in this frequency regime reduce the uniformity of the quadrature coil anyway. The advantage of head arrays is that parallel imaging methods can be used to accelerate spatial encoding of images. The result dramatically increased image quality in regions where single-shot imaging methods have historically been very poor in quality (e.g., orbitofrontal regions, mesial temporal lobe, and brainstem). Some of these brain regions have important and interesting functions. Parallel imaging techniques with the head arrays available to most researchers will typically result in lower SNR throughout most of the brain, but these can still be effectively employed in situations where image artifact severely limits experimental options.

5.2. Scan Plane

Issues with regard to scan plane are largely esthetic. However, there are some technical issues that are worth discussing here.

Perhaps the most important issue is brain tissue coverage. The scan plane of choice can affect the coverage of brain tissue. Given a TE, receiver bandwidth (RBW), and TR, the number of slices available to be acquired in one TR is fixed on a given scanner.⁶ The most efficient scan plane for acquiring most human brains is the sagittal plane. The brain in most adults is shortest in the right/left dimension, and so fewer slices will be required to cover the entire brain.

An axial acquisition plane is recommended in **Table 2** due to the fact that it is a more intuitive scan plane to work in, both anatomically and from a physics perspective. Eddy current and higher order artifacts stemming from gradient and shim coil interactions, that are essentially related to coil geometry, are more easily understood in the axial plane. With that said, it is a simple extension to understand these effects in other scan planes. Axial imaging has the added advantage over sagittal and coronal imaging planes in that lateral, frontal, prefrontal, and posterior regions of the brain can be imaged entirely within a relatively few slices (i.e., the very top and very bottom of the brain are considered by many to be more “expendable” than these other regions). The axial plane is a very common imaging choice in fMRI and thus is listed in **Table 2**.

5.3. Field-of-View

FOV has an impact on fMRI signal optimization in three ways (1) together with image matrix, it determines the in-plane voxel size and there are a number of issues with regard to this that will be outlined below, (2) image artifact reduction, particularly in the phase direction, with volume RF coils, and (3) brain coverage.

The last of these points is rather trivial; however, the other two are important with regard to general acquisition strategy.

5.3.1. In-Plane Voxel Size

In-plane voxel size affects fMRI acquisition SNR (and thus fMRI signal detection efficiency) and image quality. At lower field strengths, the SNR issue will dominate and thus it is recommended to use a larger voxel size at the expense of spatial resolution in order to enhance signal detection efficiency. Further signal enhancement can be attained with minimal loss of spatial resolution at 1.5 T through special spatial filtering techniques (76, 77).

At field strengths of 3.0 T and higher, voxel size has an interaction with physiologic noise from cardiac and respiratory sources that can be detrimental to fMRI signal detection (58). It is recommended that smaller voxels be employed at 3 T and higher

⁶There are, of course, other parameters that can affect this, such as gradient slew rate, partial Fourier, and/or field-of-view acquisition, etc.

to limit the impact on BOLD CNR from physiologic noise. If spatial resolution is not a concern, it is still recommended that data be acquired at a higher spatial resolution (i.e., smaller voxel size) and retrospective spatial filtering be employed to further increase the CNR (77).

5.3.2. Image Artifact Reduction

Due to the fact that the spatial encoding in the phase direction (i.e., the direction encoded using, for instance, the phase blipping described in **Section 2.2**) is not bandwidth limited, tissue outside of the FOV in the phase direction that experiences RF excitation will appear wrapped into the FOV with a signal intensity related to the leakage RF experienced by that tissue. For that reason, it is important for most acquisitions that the FOV in the phase direction is adequate to contain the entire brain volume and is oriented such that other tissue is not proximal to the FOV. An example would be a coronal plane acquisition with the phase-encode direction in the inferior/superior direction. In this acquisition, even if the entire brain volume is within the FOV, tissue from the neck and the trunk of the body that is within the sensitive volume of transmit and receive RF coils will appear aliased into the top of the FOV. A more common problem is that the FOV is chosen too small and one side of the brain is wrapped into the other side of the brain (**Fig. 23**). This is avoided most simply by adopting a large enough FOV in the phase direction. The recommendation in **Table 2** is sufficient for most adults.

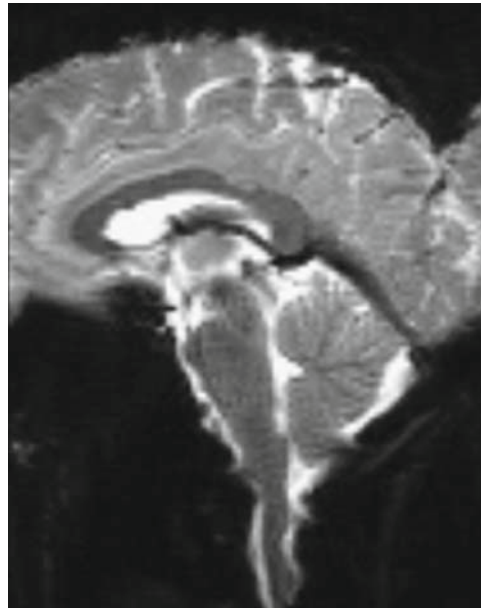


Fig. 23. Sagittal echo-planar imaging (EPI) image with phase direction too small for the brain dimension in the anterior–posterior direction. The anterior portion is phase-wrapped into the tissue at the posterior part of the brain.

5.4. Image Matrix

As stated above, the principal impact of image matrix is on voxel size and these issues are outlined above. However, it will also affect the duration of the data acquisition for a single slice in single-shot imaging. This duration, as discussed in **Section 3.1.3**, can have a detrimental effect on image quality in ultrafast imaging. Generally, the total readout time should be much less than T_2 or T_2^* . Typical methods of decreasing the scan duration while maintaining good spatial resolution are partial Fourier and partial FOV techniques, discussed briefly in **Section 2.2**. These are very commonly employed and can result in acceptable SNR tradeoffs that allow good image quality. For the 3.0-T acquisition recommended in **Table 2**, it is typical to use a partial Fourier, or partial echo, acquisition strategy. These are recommended such that reasonable SNR is maintained.

5.5. Echo Time

The TE is probably the most important consideration in optimizing a pulse sequence for BOLD contrast (or any T_2 or T_2^* contrast for that matter). As discussed in **Section 3.1**, optimal BOLD contrast is obtained by selecting a TE that is the average of the T_2 or T_2^* of the tissue in the active and inactive states. This will necessarily depend on the tissue characteristics and the field strength. The TEs recommended in **Table 2** are typical TEs for a GRE-EPI acquisition that have a reasonable balance between tissue sensitivity and specificity. Adopting a longer TE can result in less sensitivity to intravascular signal, especially at 3.0 T and higher, while a shorter TE can result in higher SNR. Ranges of TE for T_2^* BOLD imaging at 1.5 T include 40–65 ms, while ranges used experimentally at 3.0 T can range from 25 to 40 ms. One should be careful when adopting TEs outside of these ranges as BOLD contrast can be severely attenuated.

5.6. Repetition Time

With regard to BOLD contrast, TR has the fairly simple effect of increasing or lowering SNR based on the T_1 of the tissue. For a TR short with respect to the T_1 of the tissue of interest, the MR signal will be saturated. This will be discussed in some detail in the section regarding the flip angle. Here, we will simply point out that very short TRs can result a significant reduction in SNR, and can subsequently also result in a significant contribution from flow contrast, depending on the saturated state and whether a slice gap is included in the prescription.

Increased blood flow results in an apparent shortening of the T_1 relaxation time due to the effect of infusing blood on the net saturated state of the protons in a given voxel. Generally, the effect of increased flow on the T_1 of a given voxel can be expressed as

$$\frac{1}{T_{1\text{eff}}} = \frac{1}{T_1} + \frac{f}{\lambda}, \quad (5)$$

where $T_{1\text{eff}}$ is the observed T_1 in the presence of flow. λ is the tissue blood volume fraction and f is the rate of flow. Thus, an *increase* in blood flow will result in an apparent shortening of the observed T_1 in the affected brain region.

With regard to fMRI, the TR normally determines the sampling rate. This, combined with experimental design (stimulus presentation, duration, number of samples, etc.) determines the detection efficiency for BOLD signals (see also **Section 4.2.1**).

A note with regard to TR and fMRI is that sensitivity to out-of-plane motion, discussed above in **Section 3.2.1**, is a consequence of spin saturation in two-dimensional single-shot MRI. Longer TRs will lead to lower saturation, and thus lower sensitivity to out-of-plane motion.⁷

5.7. Flip Angle

Technically, the flip angle relates to the amount of RF power applied at the excitation stage of a pulse sequence. For a given tissue type (i.e., T_1) and TE, MR signal is optimized at a flip angle referred to as the Ernst angle. The formula for the Ernst angle is given by

$$\alpha_E = \cos^{-1} \left\{ \exp \left(\frac{-TR}{T_1} \right) \right\}. \quad (6)$$

Since the flip angle controls the amount of RF power transmitted to the tissue, reducing the flip angle in acquisitions with a short TR can reduce the amount of flow contribution observed in a BOLD-weighted acquisition, possibly increasing spatial specificity of detected neuronal activation.

5.8. Receiver Bandwidth

RBW, in a conventional MRI sequence, has an easily interpreted impact on images: since the RBW is essentially the speed at which the MR signal is digitized, lower bandwidth results in higher SNR, but the resulting longer data acquisition can impact image quality. With single-shot imaging techniques, the effect of RBW is not as straightforward. At low RBW, the readout window length can be long enough such that SNR is reduced. At higher RBW, the reduced artifact from shorter readout time lessens or even completely eliminates the expected reduction in SNR. It is difficult to recommend an exact RBW for these types of acquisitions, since the optimal operating point will depend on scanner hardware characteristics such as slew rate that is highly variable between scanners. The parameters indicated in **Table 2** should give reasonable results in most clinical MRI scanners. Increasing RBW can help to reduce susceptibility artifacts, such as image

⁷ More accurately, retrospective motion correction techniques will be more effective.

warping, in orbitofrontal or other regions in much the same way as discussed above under parallel imaging.

5.9. Slice Thickness

Choice of slice thickness has generally the same effect as spatial resolution mentioned earlier. Principal effects are brain coverage, SNR, and image quality. The recommended slice thickness in **Table 2** should give nearly whole-brain coverage in most adults, with acceptable SNR and image artifact given field strength limitations.

As a further note, there is no mention of a slice gap in **Table 2**. A slice gap is not recommended in fMRI studies where the entire brain is desired. The RF excitation for a given slice will not be perfect, so if a small gap (<10% of slice thickness) between slices were permitted, the tissue in this gap would still be sampled, although less than if the slices were simply made thicker. Historically, slice gaps were included to improve SNR in two-dimensional acquisition by reducing RF crosstalk between adjacent slices. The longer TR recommended in **Table 2**, along with an interleaved style pattern of slice excitation, should be sufficient to make this a negligible effect in most clinical scanners.

5.10. Number of Slices

The desired number of slices in an fMRI acquisition will affect temporal resolution and brain coverage. The recommended number of slices in **Table 2** should permit whole brain coverage in most situations. Issues with regard to TR are discussed earlier.

6. Concluding Remarks

As stated at the beginning, and illustrated throughout this chapter, there are many experimental design issues in fMRI that will affect the exact pulse sequence prescription adopted for a particular study. The intent of this chapter is to give an overview of these issues and recommend a starting point for a sequence prescription that will be generally feasible on most modern MRI scanners, along with a sense of the impact of each of the sequence features. There are two caveats with regard to the content of this chapter (1) it is strongly recommended that fMRI researchers work closely with an MR physicist experienced in fMRI when there are specific issues that may effect acquisition choices and (2) ideally, pulse sequence prescription and paradigm design should both be considered together when designing an fMRI experiment. Informing the data acquisition design based on the needs with regard to the experimental hypothesis or analysis methods is critical to a successful fMRI experiment.

References

- Belliveau JW, Kennedy DN, Jr., McKinstry RC, et al. Functional mapping of the human visual cortex by magnetic resonance imaging. *Science* 1991;254:716–719.
- Ogawa S, Lee TM, Nayak AS, Glynn P. Oxygenation-sensitive contrast in magnetic resonance image of rodent brain at high magnetic fields. *Magn Reson Med* 1990;14:68–78.
- Bandettini PA, Wong EC, Hinks RS, Tikofsky RS, Hyde JS. Time course EPI of human brain function during task activation. *Magn Reson Med* 1992;25:390–397.
- Kwong KK, Belliveau JW, Chesler DA, et al. Dynamic magnetic resonance imaging of human brain activity during primary sensory stimulation. *Proc Natl Acad Sci USA* 1992;89:5675–5679.
- Ogawa S, Tank DW, Menon R, et al. Intrinsic signal changes accompanying sensory stimulation: functional brain mapping with magnetic resonance imaging. *Proc Natl Acad Sci USA* 1992;89:5951–5955.
- Frahm J, Bruhn H, Merboldt KD, Hancic W. Dynamic MR imaging of human brain oxygenation during rest and photic stimulation. *J Magn Reson Imaging* 1992;2:501–505.
- Weisskoff RM, Davis TL. Correcting gross distortion on echo planar images, Society of Magnetic Resonance in Medicine 11th Annual Meeting, Berlin, 1992.
- Foerster BU, Tomasi D, Caparelli EC. Magnetic field shift due to mechanical vibration in functional magnetic resonance imaging. *Magn Reson Med* 2005;54:1261–1267.
- Ahn CB, Kim JH, Cho ZH. High-speed spiral-scan echo planar NMR imaging-I. *IEEE Trans Med Imaging* 1986;5:2–7.
- Bruder H, Fischer H, Reinfelder HE, Schmitt F. Image reconstruction for echo planar imaging with nonequidistant k-space sampling. *Magn Reson Med* 1992;23:311–323.
- Pipe JG, Duerk JL. Analytical resolution and noise characteristics of linearly reconstructed magnetic resonance data with arbitrary k-space sampling. *Magn Reson Med* 1995;34:170–178.
- Bornert P, Schomberg H, Aldefeld B, Groen J. Improvements in spiral MR imaging. *Magma* 1999;9:29–41.
- Glover GH, Law CS. Spiral-in/out BOLD fMRI for increased SNR and reduced susceptibility artifacts. *Magn Reson Med* 2001;46:515–522.
- Preston AR, Thomason ME, Ochsner KN, Cooper JC, Glover GH. Comparison of spiral-in/out and spiral-out BOLD fMRI at 1.5 and 3 T. *Neuroimage* 2004;21:291–301.
- Sodickson DK, Manning WJ. Simultaneous acquisition of spatial harmonics (SMASH): fast imaging with radiofrequency coil arrays. *Magn Reson Med* 1997;38:591–603.
- Pruessmann KP, Weiger M, Scheidegger MB, Boesiger P. SENSE: sensitivity encoding for fast MRI. *Magn Reson Med* 1999;42:952–962.
- Griswold MA, Jakob PM, Heidemann RM, et al. Generalized autocalibrating partially parallel acquisitions (GRAPPA). *Magn Reson Med* 2002;47:1202–1210.
- Heidemann RM, Griswold MA, Kiefer B, et al. Resolution enhancement in lung 1H imaging using parallel imaging methods. *Magn Reson Med* 2003;49:391–394.
- Ohliger MA, Grant AK, Sodickson DK. Ultimate intrinsic signal-to-noise ratio for parallel MRI: electromagnetic field considerations. *Magn Reson Med* 2003;50:1018–1030.
- Wiesinger F, Boesiger P, Pruessmann KP. Electrodynamics and ultimate SNR in parallel MR imaging. *Magn Reson Med* 2004;52:376–390.
- Blaimer M, Breuer F, Mueller M, Heidemann RM, Griswold MA, Jakob PM. SMASH, SENSE, PILS, GRAPPA: how to choose the optimal method. *Top Magn Reson Imaging* 2004;15:223–236.
- Ohliger MA, Sodickson DK. An introduction to coil array design for parallel MRI. *NMR Biomed* 2006;19:300–315.
- Pruessmann KP, Weiger M, Bornert P, Boesiger P. Advances in sensitivity encoding with arbitrary k-space trajectories. *Magn Reson Med* 2001;46:638–651.
- Weiger M, Pruessmann KP, Osterbauer R, Bornert P, Boesiger P, Jezzard P. Sensitivity-encoded single-shot spiral imaging for reduced susceptibility artifacts in BOLD fMRI. *Magn Reson Med* 2002;48:860–866.
- Heidemann RM, Griswold MA, Seiberlich N, et al. Direct parallel image reconstructions for spiral trajectories using GRAPPA. *Magn Reson Med* 2006;56:317–326.
- Griswold MA, Kannengiesser S, Heidemann RM, Wang J, Jakob PM. Field-of-view limitations in parallel imaging. *Magn Reson Med* 2004;52:1118–1126.
- Griswold MA, Breuer F, Blaimer M, et al. Autocalibrated coil sensitivity estimation for parallel imaging. *NMR Biomed* 2006;19:316–324.

28. Sodickson DK. Tailored SMASH image reconstructions for robust in vivo parallel MR imaging. *Magn Reson Med* 2000;44:243–251.
29. Sanchez-Gonzalez J, Tsao J, Dydak U, Desco M, Boesiger P, Paul Pruessmann K. Minimum-norm reconstruction for sensitivity-encoded magnetic resonance spectroscopic imaging. *Magn Reson Med* 2006;55:287–295.
30. Lin FH, Kwong KK, Belliveau JW, Wald LL. Parallel imaging reconstruction using automatic regularization. *Magn Reson Med* 2004;51:559–567.
31. Block KT, Frahm J. Spiral imaging: a critical appraisal. *J Magn Reson Imaging* 2005;21:657–668.
32. Tsao J, Boesiger P, Pruessmann KP. k - t BLAST and k - t SENSE: dynamic MRI with high frame rate exploiting spatiotemporal correlations. *Magn Reson Med* 2003;50:1031–1042.
33. Huang F, Akao J, Vijayakumar S, Duensing GR, Limkeman M. k - t GRAPPA: a k -space implementation for dynamic MRI with high reduction factor. *Magn Reson Med* 2005;54:1172–1184.
34. Cuppen JJ, Groen JP, Konijn J. Magnetic resonance fast Fourier imaging. *Med Phys* 1986;13:248–253.
35. Noll DC, Nishimura DG, Macovski A. Homodyne detection in magnetic resonance imaging. *IEEE Trans Med Imaging* 1991;10:154–163.
36. Jesmanowicz A, Bandettini PA, Hyde JS. Single-shot half- k -space high-resolution gradient-recalled EPI for fMRI at 3 Tesla. *Magn Reson Med* 1998;40:754–762.
37. Hyde JS, Biswal BB, Jesmanowicz A. High-resolution fMRI using multislice partial k -space GR-EPI with cubic voxels. *Magn Reson Med* 2001;46:114–125.
38. Meyer CH, Pauly JM, Macovski A, Nishimura DG. Simultaneous spatial and spectral selective excitation. *Magn Reson Med* 1990;15:287–304.
39. Zhou XJ, Du YP, Bernstein MA, Reynolds HG, Maier JK, Polzin JA. Concomitant magnetic-field-induced artifacts in axial echo planar imaging. *Magn Reson Med* 1998;39:596–605.
40. Reeder SB, Atalar E, Faranesh AZ, McVeigh ER. Referenceless interleaved echo-planar imaging. *Magn Reson Med* 1999;41:87–94.
41. Duyn JH, Yang Y, Frank JA, van der Veen JW. Simple correction method for k -space trajectory deviations in MRI. *J Magn Reson* 1998;132:150–153.
42. Yudilevich E, Stark H. Spiral sampling in magnetic resonance imaging—the effect of inhomogeneities. *IEEE Trans Med Imaging* 1987;6:337–345.
43. Jezzard P, Balaban RS. Correction for geometric distortion in echo planar images from B_0 field variations. *Magn Reson Med* 1995;34:65–73.
44. Blamire AM, Rothman DL, Nixon T. Dynamic shim updating: a new approach towards optimized whole brain shimming. *Magn Reson Med* 1996;36:159–165.
45. Wilson JL, Jenkinson M, de Araujo I, Kringelbach ML, Rolls ET, Jezzard P. Fast, fully automated global and local magnetic field optimization for fMRI of the human brain. *Neuroimage* 2002;17:967–976.
46. Ward HA, Riederer SJ, Jack CR, Jr. Real-time autoshimming for echo planar time-course imaging. *Magn Reson Med* 2002;48:771–780.
47. Yang QX, Williams GD, Demeure RJ, Mosher TJ, Smith MB. Removal of local field gradient artifacts in T_2^* -weighted images at high fields by gradient-echo slice excitation profile imaging. *Magn Reson Med* 1998;39:402–409.
48. Constable RT, Spencer DD. Composite image formation in z -shimmed functional MR imaging. *Magn Reson Med* 1999;42:110–117.
49. Chen N, Wyrwicz AM. Removal of intravoxel dephasing artifact in gradient-echo images using a field-map based RF refocusing technique. *Magn Reson Med* 1999;42:807–812.
50. Oesterle C, Markl M, Strecker R, Kraemer FM, Hennig J. Spiral reconstruction by regridding to a large rectilinear matrix: a practical solution for routine systems. *J Magn Reson Imaging* 1999;10:84–92.
51. Moriguchi H, Duerk JL. Modified block uniform resampling (BURS) algorithm using truncated singular value decomposition: fast accurate gridding with noise and artifact reduction. *Magn Reson Med* 2001;46:1189–1201.
52. Nehrke K, Bornert P. Prospective correction of affine motion for arbitrary MR sequences on a clinical scanner. *Magn Reson Med* 2005;54:1130–1138.
53. Hajnal JV, Myers R, Oatridge A, Schwieso JE, Young IR, Bydder GM. Artifacts due to stimulus correlated motion in functional imaging of the brain. *Magn Reson Med* 1994;31:283–291.
54. Friston KJ, Williams S, Howard R, Frackowiak RS, Turner R. Movement-related effects in fMRI time-series. *Magn Reson Med* 1996;35:346–355.
55. Bullmore ET, Brammer MJ, Rabe-Hesketh S, et al. Methods for diagnosis and treatment of

- stimulus-correlated motion in generic brain activation studies using fMRI. *Hum Brain Mapp* 1999;7:38–48.
56. Jezzard P, LeBihan D, Cuenod D, Pannier L, Prinster A, Turner R. An investigation of the contribution of physiological noise in human functional MRI studies at 1.5 Tesla and 4 Tesla, Society of Magnetic Resonance in Medicine 12th Annual Meeting, New York, NY, 1992.
 57. Lowe MJ, Mock BJ, Sorenson JA. Functional connectivity in single and multislice echoplanar imaging using resting-state fluctuations. *Neuroimage* 1998;7:119–132.
 58. Triantafyllou C, Hoge RD, Krueger G, et al. Comparison of physiological noise at 1.5 T, 3 T and 7 T and optimization of fMRI acquisition parameters. *Neuroimage* 2005;26:243–250.
 59. Friedman L, Glover GH. Report on a multicenter fMRI quality assurance protocol. *J Magn Reson Imaging* 2006;23:827–839.
 60. Fu ZW, Wang Y, Grimm RC, et al. Orbital navigator echoes for motion measurements in magnetic resonance imaging. *Magn Reson Med* 1995;34:746–753.
 61. Lee CC, Jack CR, Jr., Grimm RC, et al. Real-time adaptive motion correction in functional MRI. *Magn Reson Med* 1996;36:436–444.
 62. Thesen S, Heid O, Mueller E, Schad LR. Prospective acquisition correction for head motion with image-based tracking for real-time fMRI. *Magn Reson Med* 2000;44:457–465.
 63. Zhao X, Bodurka J, Jesmanowicz A, Li SJ. B(0)-fluctuation-induced temporal variation in EPI image series due to the disturbance of steady-state free precession. *Magn Reson Med* 2000;44:758–765.
 64. Raj D, Anderson AW, Gore JC. Respiratory effects in human functional magnetic resonance imaging due to bulk susceptibility changes. *Phys Med Biol* 2001;46:3331–3340.
 65. Dagli MS, Ingeholm JE, Haxby JV. Localization of cardiac-induced signal change in fMRI. *Neuroimage* 1999;9:407–415.
 66. Bhattacharyya PK, Lowe MJ. Cardiac-induced physiologic noise in tissue is a direct observation of cardiac-induced fluctuations. *Magn Reson Imaging* 2004;22:9–13.
 67. Guimaraes AR, Melcher JR, Talavage TM, et al. Imaging subcortical auditory activity in humans. *Hum Brain Mapp* 1998;6:33–41.
 68. Hu X, Le TH, Parrish T, Erhard P. Retrospective estimation and correction of physiological fluctuation in functional MRI. *Magn Reson Med* 1995;34:201–212.
 69. Glover GH, Li TQ, Ress D. Image-based method for retrospective correction of physiological motion effects in fMRI: RET-ROICOR. *Magn Reson Med* 2000;44:162–167.
 70. Beall EB, Lowe MJ. Isolating physiologic noise sources with independently determined spatial measures. *Neuroimage* 2007;37:1286–1300.
 71. Stefanovic B, Pike GB. Human whole-blood relaxometry at 1.5 T: Assessment of diffusion and exchange models. *Magn Reson Med* 2004;52:716–723.
 72. Friston KJ, Holmes AP, Worsley KJ, Poline J-B, Frith CD, Frackowiak R. Statistical parametric mapping in functional imaging: A general linear approach. *Hum Brain Mapp* 1995;2:189–210.
 73. Josephs O, Turner R, Friston KJ. Event-related fMRI. *Hum Brain Mapp* 1997;5:243–248.
 74. Bandettini PA, Jesmanowicz A, Wong EC, Hyde JS. Processing strategies for time-course data sets in functional MRI of the human brain. *Magn Reson Med* 1993;30:161–173.
 75. Miezin FM, Maccotta L, Ollinger JM, Petersen SE, Buckner RL. Characterizing the hemodynamic response: effects of presentation rate, sampling procedure, and the possibility of ordering brain activity based on relative timing. *Neuroimage* 2000;11:735–759.
 76. Lowe MJ, Sorenson JA. Spatially filtering functional magnetic resonance imaging data. *Magn Reson Med* 1997;37:723–729.
 77. Triantafyllou C, Hoge RD, Wald LL. Effect of spatial smoothing on physiological noise in high-resolution fMRI. *Neuroimage* 2006;32:551–557.



<http://www.springer.com/978-1-60327-918-5>

fMRI Techniques and Protocols

Filippi, M. (Ed.)

2009, XIII, 843 p., Hardcover

ISBN: 978-1-60327-918-5

A product of Humana Press